McKelvey School of Engineering Theses & Dissertations

McKelvey School of Engineering

Winter 12-12-2023

Commercial adsorbents for CO2 Removal for Biogas Upgradation: An Experimental Study

Aakriti Bagla
Washington University – McKelvey School of Engineering

WASHINGTON UNIVERSITY IN ST. LOUIS

McKelvey School of Engineering
Department of Energy, Environmental and Chemical Engineering

Thesis Examination Committee:
Benjamin Kumfer, Chair
Jason He
Xinhua Liang

Commercial Adsorbents for CO_2 Removal for Biogas Upgradation:
An Experimental Study
by
Aakriti Bagla

A thesis presented to
the McKelvey School of Engineering
of Washington University in
partial fulfillment of the
requirements for the degree
of Master of Science

December 2023
St. Louis, Missouri

Table of Contents

List of Figures

List of Tables

Nomenclature

Å	Angstrom
ANG	Adsorptive storage of natural gas
°C	Celsius
cc	Cubic centimeter
H_2	Hydrogen
H_2S	Hydrogen sulfide
K_1	Adsorption rate constant
K_2	Desorption rate constant
K_{AB}	Adam Bohart rate constant
K_{Th}	Thomas rate constant
K_{YN}	Yoon Nelson rate constant
kWh/Nm^3	Kilowatt hour per cubic meter
m	Mass of adsorbent
mmol	Milli moles
MPa	Mega Pascal
N_2	Nitrogen Gas
NH_3	Ammonia
N_o	Adsorption capacity of the adsorbent per unit volume of the bed
nm	Nano meters
O_2	Oxygen
ppm	Parts per million
PSIG	Pound-force per square inch

p_L	Langmuir pressure
Q	Volumetric flowrate
sccm	Standard cubic centimeter per minute
STP	Standard temperature and pressure
τ	Time required for 50% breakthrough
V_{eff}	Effective volume
θ	Covered surface

<u>Acknowledgments</u>

ABSTRACT OF THE THESIS

Commercial Adsorbents for CO_2 Removal for Biogas Upgradation:

An Experimental Study

by

Aakriti Bagla

Master of Science in Energy, Environmental and Chemical Engineering

Washington University in St. Louis, 2023

Professor Benjamin Kumfer, Chair

The world's limitless energy demands and the need to reduce carbon emissions are both addressed by biogas, an easily accessible renewable energy source. Theoretically, compared to gasoline, the use of biogas or biomethane—which is more than 90% methane after carbon dioxide removal—for transportation purposes can reduce GHG emissions by 60% to 80%. With the goal of understanding their effectiveness and their potential to adsorb carbon dioxide from a gas mixture of 1:1 CO_2 & N_2 at STP conditions, this study undertook a thorough investigation of commonly used commercial adsorbents, including activated carbon, zeolites, and metal oxides, An in-depth method was used to determine the specific surface area of these microporous adsorbents after studying their textural characteristics. The research entails the development of an experimental setup tailored for the exploration of vacuum pressure swing adsorption (VPSA), temperature swing adsorption (TSA), and a combination of both methodologies to determine adsorption capacity pre & post-regeneration. The primary objectives of the study are twofold: firstly, to identify a set of adsorbents capable of effectively removing contamination, specifically CO_2, from biogas. This involves a comprehensive comparison of their textural characteristics, breakthrough curves, and adsorption capacities. Secondly, the research aims to investigate the

regeneration of these adsorbents, seeking to comprehend the optimal processes for future

application of certain materials. Through this endeavor, the study contributes valuable insights

into the selection and regeneration of adsorbents for biogas upgradation

Chapter 1

Motivation and Objective

The primary factors influencing the energy policies of nations worldwide today are energy security, economic growth, and environmental protection. According to the projections made by the World Energy Forum, it is anticipated that the depletion of fossil fuel reserves, including oil, coal, and gas, will occur within the next ten decades. This depletion is primarily attributed to a substantial increase in global energy demand, which is expected to multiply by a factor of two or three throughout the course of this century.[1] In light of increasing energy demand and greenhouse gas emissions, international treaties such as the Kyoto Protocol and Agenda 21 place a strong emphasis on the development and utilization of renewable energy sources.[2]

Biogas is an easy-to-reach, renewable energy source that could help meet the world's endless energy needs and cut down on carbon emissions at the same time. It is thought that using upgraded biogas or biomethane (>90% methane) for transportation can cut greenhouse gas (GHG) emissions by 60% to 80% compared to petrol. This depends on the feedstock that is used.[3,4] It consists mainly of methane (CH_4) and carbon dioxide (CO_2), which are generated through the anaerobic fermentation of organic substances within an anaerobic digester. Organic matter encompasses a range of materials, including municipal waste, manure, sewage waste, and other biodegradable feedstocks. When biogas undergoes adequate purification, it exhibits similar characteristics to natural gas. The combustion of natural gas yields a lower amount of carbon dioxide and a higher amount of water vapor per unit of energy compared to the combustion of coal, gasoline or diesel.[5,6]

Biogas typically has a calorific value of 21.5 MJ/m^3, while natural gas has a calorific value of 35.8 MJ/m^3.[7] The incombustible portion of biogas, primarily CO_2, is primarily responsible for the difference in calorific values between the two. Because biogas contains large portion of CO_2, it loses some of its heating value and costs more to compress and transport. This makes it less economically viable to use biogas to make electricity right where it is produced. Likewise, the presence of additional contaminants in biogas can have a negative impact on downstream equipment structure, leading to corrosion of boiler and engine tubes as well as steel chimneys. Carbon dioxide and methane are the primary components of biogas. Furthermore, it includes trace amounts of other gases, including hydrogen, nitrogen, and hydrogen sulfide. The differences in contamination between landfill gas, natural gas, and biogas are listed in Table 1. The table shows that the primary distinction between natural gas and biogas is the latter's lower concentration of hydrocarbons and higher concentration of CO_2. Because of these variations, biogas has less energy per unit volume than natural gas.[8,9] Once these impurities are taken out, the upgraded gas will contain high-quality methane and can be used for more things, like fueling vehicles or making heat and electricity.[10]

Table 1: Contaminations in biogas, natural gas and landfill gas[8]

Gas	Biogas	Landfill gas	Natural gas
CH_4 (% vol)	90-70	~65	~90
CO_2 (%vol)	30-40	15-50	1
Hydrocarbons (%vol)	0	0	9
H_2 (%vol)	0	0-3	0
N_2 (%vol)	~0.2	5-40	~0.3
O_2 (%vol)	0	0-5	0

	0-4000	0-100	3
H$_2$S (ppm)	0-4000	0-100	3
NH$_3$ (ppm)	100	5	0
Heating value, kWh/Nm^3	~6.5	~4.4	~11.0

There are currently a number of technologies available for biogas upgradation, including, adsorption, absorption and membrane-based gas permeation. Additionally, developments are being made in the fields of novel technologies such as hybrid membrane-cryogenic technologies, in situ methane enrichment.[11] But just as with solar and wind power, there are challenges in the production and use of biogas. These primarily include high operating costs, energy-intensive processes, and insufficient policy support. Given the possibility of increased market competition in the future, there is a need to develop new biogas upgrading technologies and optimize existing ones in order to reduce operating costs and use less energy in biogas production.[11]

Processes that are based on adsorption and make use of microporous materials are an extremely promising and cost-efficient technology. When performing a Pressure Swing Adsorption (PSA)/ Vacuum Swing Adsorption (VSA) process, the adsorbent is regenerated by reducing the pressure or increasing the vacuum respectively. On the other hand, when performing a Temperature Swing Adsorption (TSA) operation, the regeneration is carried out by increasing the temperature.[12] PSA/VSA is widely regarded as the most appealing and efficient biogas upgrading process due to its simple control, low operating and capital investment costs, and higher energy efficiency.[13–17]

In this study, a comprehensive investigation is conducted on commonly employed commercial adsorbents, namely activated carbon, zeolites, and metal oxides, using CO$_2$ and N$_2$ with the aim

3

of comprehending their effectiveness and the potential for regeneration through the above-mentioned adsorption processes. The analysis of the textural characteristics of adsorbents, in conjunction with the evaluation of breakthrough curves derived from experimental setup, offers valuable insights into the most suitable adsorption procedures to be employed for both commercially available adsorbents and newly synthesized ones; for removing CO_2 to upgrade biogas. Within the scope of this research study, the methodology described below is chosen in order to achieve aforementioned objectives.

1. Review of the existing literature:

An extensive examination of existing literature to identify appropriate adsorbents for effectively eliminating significant levels of contamination, specifically carbon dioxide, from biogas.

Choosing three commonly found adsorbents—activated carbon, magnesium oxide, and zeolite 13X—after analyzing information from the literature review.

2. Adsorbent characterization:

Study of gas equilibrium models and examining the textural properties of the chosen adsorbents to better understand how they interact with the adsorbate.

An extensive procedure for determining the specific surface area and pore size of microporous adsorbents through the utilization of BET analysis.

3. Methodology:

A laboratory apparatus to carry out vacuum pressure swing adsorption and temperature swing adsorption.

Investigating the dynamic interaction between a mixture of CO_2 and N_2 gases using the selected adsorbents.

4. Breakthrough Curve Analysis:

Analyzing breakthrough curves obtained from the experimental study, correlating them with the textural properties of the adsorbents.

Assessing the adsorption capacity of each adsorbent, establishing guidelines for comparative analysis.

5. Process Summary and Recommendations:

Developing a comprehensive process summary for upgrading biogas, with the initial step involving the removal of CO_2.

Recommending adsorbents deemed suitable for the identified process based on the evaluation of their adsorption capacities and characteristic curves.

Chapter 2

Introduction

2.1 Adsorbents

The most crucial feature of an adsorbent is its adsorption capacity, also referred to as "loading." The amount of adsorbate absorbed by the adsorbent per unit mass (or volume) of the adsorbent is its simple definition. It is dependent upon temperature, fluid-phase concentration, and other factors (particularly the adsorbent's initial state). Adsorption capacity data are typically collected as an isotherm (loading versus concentration at constant temperature) at different adsorbate concentrations (or partial pressures for vapors or gases). Because it determines the amount of adsorbent needed and fixes the volume of the adsorber vessels—both of which are typically significant, if not dominant—adsorption capacity is crucial to the capital cost.).[18]

Another crucial attribute to consider when choosing an adsorbent, particularly in the context of biogas, is the adsorbent's selectivity with regard to CO_2 adsorption. In the context of CO_2 separation from a CH_4/CO_2 mixture, an optimal adsorbent must possess distinct adsorption characteristics for the two gases, i.e., it must adsorb carbon dioxide preferentially while leaving a large proportion of methane molecules in the gaseous state. The similar kinetic diameters of the two molecules (0.330 nm for CO_2 and 0.382 nm for CH_4) make the design of kinetic-based adsorbents extremely challenging. Nevertheless, a significant disparity in polarity exists between the two substances. CO_2 possesses a quadrupolar moment, whereas CH_4 is classified as a non-

polar molecule. Adsorbate–adsorbent interactions are strengthened, which leads to an increased selectivity towards carbon dioxide in the presence of polar surface functionalities.[19]

2.1.1 Zeolites

Zeolites, crystalline aluminosilicate materials comprised of alkali or alkali earth elements such as sodium, potassium, and calcium, exhibit a well-defined structure with tetrahedra of silicon and aluminum forming the primary structural units. The stoichiometric formula, $Mx/n[(AlO_2)x(SiO_2)y]zH_2O$, details the arrangement, where x and y are integers, n is the cation M valence, and z is the water molecules in each unit cell. Approximately 150 types of zeolites, designated by letters, have been synthesized, each possessing unique characteristics.[20]

Table 1.2 Types of zeolites and their properties.[21–24]

Zeolite Type	Feed mixture	Feed condition	Adsorption capacity
NaUSY	58% CH_4 + 42% CO_2	STP	11−15 mol methane/kg
Zeolite 5A	60% CH_4 + 40% CO_2	6 bar	4.49 mol of CO_2/kg
Zeolite 13X	60% CH_4 + 40% CO_2	1 bar	4.6 mmol of CO_2/g
ZSM-5	50% CH_4 + 50% CO_2	1 bar	1.6 mmol/g CO_2

2.1.2 Activated carbon

Activated carbons are the adsorbents with the most favorable characteristics for ANG storage, because they have a large microporous volume, are efficiently compacted into a packed bed, and can be cheaply manufactured in large quantities The enhanced storage results from gas adsorption into the micropores. The activation process to develop microporosity in the carbon matrix creates a very high surface area formed by an intricate network of small pores, where the

density of the adsorbed phase is liquid-like, thus providing for a higher storage density than is possible by compression alone. The storage density enhancement factors achieved by ANG range from 2 to 10, depending on the operating pressure.[25]

2.1.3 Metal Oxide

Magnesium oxide (MgO) is a white, crystalline powder with a high chemical stability and thermal resistance It has a high basicity and can effectively neutralize acidic gases, making it a potential adsorbent for CO2 removal in biogas production [26]Solid commercial magnesium oxide is available in various particle sizes and morphologies, with surface area and pore size distribution affecting its adsorption performance.

Mineral oxides like magnesium oxide (MgO) have gotten a lot of research attention because they can capture CO2 by making magnesium carbonate ($MgCO_3$) at different temperatures. At low temperatures, MgO turns into unidentate $MgCO_3$ and bidentate $MgCO_3$ at high temperatures. The rate at which $MgCO_3$ is formed depends on the temperature, the saturation state of the Mg^{2+} species, and the partial pressure of CO_2. As low as 60°C, MgO can both physically and chemically absorb CO_2. This can happen either with water vapor present or without.[27]

These mesoporous MgO is excellent for adsorbing CO_2, but the entire desorption of adsorbed CO_2 can only be achieved by heating for a long time at 450 °C, which was found to take a long time. As a result, adsorbed CO_2 can be recovered at different high temperatures, and at 800°C, a complete and sharp recovery of CO_2 is there. The capacity to absorb CO_2 increases as the temperature rises.[28]

2.2 Industrial adsorption processes

2.2.1 Vacuum pressure swing adsorption

The Vacuum Pressure Swing Adsorption (VPSA) process is a commonly employed industrial unit operation for the separation of gas mixtures. In this process, one or more gases are selectively adsorbed at high pressures and then desorbed at lower pressures.[29] The PSA and VPSA methods exhibit similarities, with the key distinction being that the VPSA method incorporates a vacuum pump to facilitate the desorption process of the adsorbate under vacuum conditions. Furthermore, it's a dry process that doesn't require any contact with water or contamination, which makes it adaptable and simple to use.

2.2.2 Temperature swing adsorption

Temperature swing adsorption (TSA) processes depend on the cyclic variation of the temperature within a bed of adsorbent material. Adsorption takes place at low temperatures, while bed regeneration occurs at high temperatures. Various methods like using steam, electrical heat tapes and others can be employed to provide temperature swing adsorption. This particular method is favored over pressure swing adsorption (PSA) when dealing with highly adsorbed species that cannot be efficiently regenerated solely through pressure adjustments. The majority of TSA processes primarily involve the utilization of direct heating methods. In the scenario of utilizing steam for direct heating, it is necessary to dry the adsorbent subsequent to the process of regeneration. In addition, it is necessary to employ a secondary unit for the purpose of separating water if the adsorbate exhibits miscibility with water. The utilization of the hot gas technique results in a desorbed phase that is diluted, requiring achieving of low condensation temperatures in order to facilitate the reuse of the adsorbate.[30] This is the rationale behind the development of

various alternative processes that aim to circumvent direct heating, which have emerged in recent times.

Chapter 3

Gas adsorption equilibrium

3.1 Introduction to adsorption equilibrium and isotherm

Adsorption primarily involves a porous solid media on which target molecules in a gas or liquid are drawn and then adhere via physical or chemical bonding. Because of the porous solid medium's extremely minute pore size, adsorbate molecules must navigate the micropore volume. Adsorbents with small pore size, moderate porosity, high micropore volume, and a network of large pores that allow molecules to flow into the adsorbent's interior are conducive to successful adsorption. The solid porous medium has a large micropore volume, resulting in a high adsorption capacity.[31–34] Given that the adsorbent is essential to the adsorption process, its adsorption capacity and kinetics must be favorable.[32] Furthermore, the information on adsorption equilibria is important data to understand adsorption process. Understanding the adsorption equilibrium of purified components is critical in evaluating the solid adsorbent's capacity to accommodate these components, regardless of the quantity of components present in the system.[34]

Adsorption isotherms characterize the equilibrium behavior of adsorptive materials at constant temperature. It is dependent on the species that are adsorbed, the adsorbent, and a number of physical characteristics of the solution, such as temperature, ionic strength, and pH.[35] They are typically established when there is a contact between the adsorbent and the adsorbate for a

11

substantial amount of time. During this time, the adsorbate concentration in the bulk solution and the interface concentration should be in dynamic balance. They are primarily used to characterize the porous solids (adsorbent) and design the industrial adsorption process.[36]

According to the IUPAC recommendation[37], it is practical to categorize pores in the context of physisorption as follows:

(i) macropores have widths greater than 50 nm;

(ii) mesopores have widths between 2 nm and 50 nm; and

(iii) micropores have widths less than 2 nm.

Micropores that are very small (about 0.7 nm wide) are called ultra micropores.

3.2 Types of adsorption isotherm

The isotherm can be shown as a curve that plots the amount of adsorbate adsorbed onto the adsorbent against either the concentration (for liquids) or the pressure (for gases) at constant temperature. The entire volume that is accessible within micropores can be considered the adsorption space. After the first layer of molecules adhere to the surface, a process known as micropore filling takes place, which is different from surface coverage that happens on the walls of open macropores or mesopores. The interpretation of the adsorption isotherm solely in terms of surface coverage is erroneous when considering micropore filling. The process of micropore filling can be considered as a fundamental physisorption mechanism.
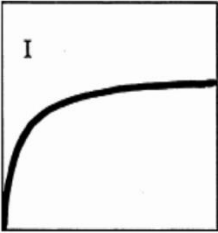
Physisorption in mesopores takes place in three more or less distinct stages. In monolayer adsorption, all of the adsorbed molecules come into contact with the adsorbent's surface layer. In
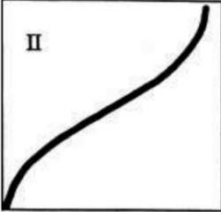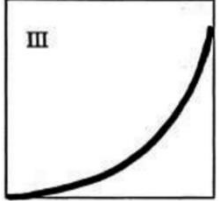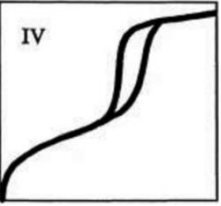
multilayer adsorption, not every layer of molecules adsorbed is in direct contact with the adsorbent surface because the adsorption space can hold multiple layers of molecules. Pore condensation occurs subsequent to multilayer adsorption within mesopores.
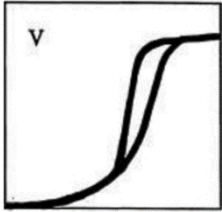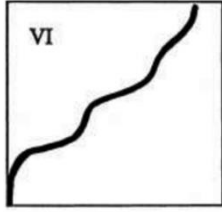
The process by which a gas condenses to a liquid-like phase in a pore at a pressure p less than the saturation pressure p° of the bulk liquid is known as capillary (or pore) condensation; in other words, capillary condensation represents a vapor-liquid phase transition in a finite-volume system. Micropore filling is not a vapor-liquid phase transition and therefore should not be referred to as capillary (or pore) condensation.[38]

Adsorption isotherms can be classified into six different groups in accordance with the IUPAC (International Union of Pure and Applied Chemistry) classification, which is determined by the isotherm shape of adsorbate-adsorbate pairs as shown in Table 2.[36]

Table 2 Classification of adsorption isotherm by IUPAC

Isotherm Type	Description	Example	Sample Graph[32]
Type I isotherms (Convex upward)[32,38–40]	Rapid adsorption at relative low pressure followed by sharp turn of isotherm. Found in Microporous materials without any mesopores or macropores.	Adsorption of water vapor on zeolite, adsorption of hydrogen on charcoal.	

13

Type II isotherms[36,39,41,42]	Positive curvature at relative low pressure. It indicated initial adsorption at energetically more favored site before being allocated to less energetically favored sites.	Adsorption of nitrogen on silica gel or iron catalyst, adsorption of water vapor on polymer-based adsorbent	
Type III isotherms (concave upward)[32,36,38,40,43]	This type occurs where the adsorbate–adsorbate interaction is big compared to adsorbate–sorbent interaction.	Adsorption of water on hydrophobic zeolites and activated carbon, adsorption of bromine and iodine on silica gel, carbon tetrachloride adsorption on mesoporous gel	
Type IV isotherms[32,38,43]	At higher pressures the slope shows increased uptake of adsorbate as pores become filled, inflection point typically occurs near completion of the first monolayer. It has 2 inflection points.	Adsorption of humid air, water vapors on specific types of activated carbon, adsorption of benzene on iron oxide and on silica gel.	

| Type V isotherms[32,38,40] | This type indicates the presence of mesopores in phase changes such as pore condensation. There is a single point of inflection. | Adsorption of water on carbon molecular sieves and on activated carbon fiber. | |
| Type VI isotherms[31,32,38] | Layers become more pronounced at low temperatures, and the isotherms present stepwise multilayer adsorbates. It has several points of inflection. | Adsorption of noble gases on the surfaces of planar graphite, and adsorption of butanol on aluminum silicate, adsorption of CH4 on MgO | |

Hysteresis loops have been observed in various IUPAC classified isotherms, as Table 1 illustrates. This suggests the presence of mesoporous material where adsorption with capillary condensation occurred.[44] The primary cause of the hysteresis is thought to be the relative vapor pressure during pore filling, which should be greater than that during pore evaporation, according to independent domain theory.[45] The network theory states that the pore-blocking effect may contribute to hysteresis.[46]

The micropore materials, which have fine pores, exhibit a Type I isotherm. In this case, adsorption occurs through either chemisorption or physisorption. Macroporous materials, denoted by Types II and III isotherms, exhibit a high and a low adsorption energy, respectively. The materials' mesoporosity is responsible for the hysteresis observed in types IV and V

isotherms, which have low and high adsorption energies, respectively.[47,48] Lastly, the type VI

isotherm, which is temperature and system dependent, characterizes the layer-by-layer

adsorption on nonporous, uniform surfaces.[48,49]

3.3 Adsorption isotherm models

3.3.1 The Langmuir Model (Two parameter model)

This model is based on a kinetic point of view, that equals the rate of adsorption to the rate of desorption from the surface at equilibrium.[44]

The Langmuir adsorption isotherm equation is defined as:

$$V = V_L \left(\frac{p}{p+p_L}\right) \qquad (1)$$

where V is the adsorbed volume, p is the absolute pressure, V_L is maximum sorption capacity and p_L is the Langmuir pressure. For quantifying the relationship between pressure and adsorbed gas in biogas, the model's simplicity facilitated its rapid adoption. But model is based on numerous assumptions thus limiting the power of predictability of the model.

Assumptions of Langmuir Model

I. Adsorbate is assumed to have homogeneous surface[50], that is adsorption energy is constant at all sites.

II. Linear relationship between pressure and volume of adsorbed gas at pressure lower than 5MPa.[51] At high pressure, Langmuir model fails to fit experimental data.

III. Monolayer adsorption phenomenon, that is there is just one adsorption site where a gas molecule is adsorbed, and no other molecules can sit on top of it.

IV.   The lateral interactions between neighboring molecules are considered to be

insignificant in the Langmuir model. This suggests that the adsorption heat is

constant and that the total amount of gas adsorbed has no impact on it. This

assumption makes sense in terms of micropores because adsorbed molecules are

comparatively far apart from one another.[52]

V.   The maximum amount of gas adsorbed is assumed to be constant under

isothermal conditions and is solely dependent on pressure in this model.[53]

Assuming above, at equilibrium, the rate of adsorption $K_1(1 - \theta)$ = rate of desorption $K_2(\theta)$.

The rate at which adsorbate molecules adsorb at the surface is proportional to the fraction of

uncovered area *(1−θ)*, while the rate at which they desorb is proportional to the covered surface

(θ).[54]

$$K_1(1 - \theta) = K_2(\theta) \qquad (2)$$

$$\text{or, } \theta = \frac{K_1 P}{K_2 + K_2 P} \qquad (3)$$

$$\text{or, } \theta = \frac{K_L P}{1 + K_L P} \qquad (4)$$

where, Langmuir constant $K_L = K_1/K_2$. Also, surface coverage can be written as the ratio of

adsorbed amount q to the maximum amount q_m that can be adsorbed by the adsorbent, that is

$\theta = \frac{q}{q_m}$.

Thus, final form of Langmuir equation becomes, $q = q_m \frac{K_L P}{1 + K_L P}$, $\qquad (5)$

Below two cases can be drawn from above equation,

• When the pressure is very low → $1 \gg K_L\,P$ → the isotherm reduces to the Henry Law: that is,

the amount adsorbed increases linearly with the pressure and can be written as: $q=q_m K_H P$, where

K_H is the Henry's law constant.

• When the pressure is relatively high → $K_L\,P \gg 1$ → the amount adsorbed reaches the

saturation capacity, all sites are occupied (is called monolayer coverage).

3.3.2 The BET (Brunauer, Emmett and Teller) Model

The BET model is extended form of Langmuir model, for multi-layer adsorption. The model

incorporates the same assumptions as the Langmuir model, while also introducing additional

simplified assumptions, namely: Similar adsorption energies are observed in the second, third,

and subsequent layers. This energy is equivalent to the fusion heat, which is unaffected by the

adsorbent-adsorbate interactions. However, the initial layer exhibits distinct energy levels

compared to the subsequent layers. As the concentration approaches the saturation concentration,

the number of layers tends towards infinity.[55]

It is widely used in multilayer adsorption system with relative pressure ranging from 0.05 to

0.30, where monolayer coverage occurs around 0.5 to 0.15 relative pressure; to find adsorbent's

surface area by using nitrogen as adsorbate.

Derivation of BET Equation

Let $A(g)$ be adsorbate and S represents adsorbent, while AS is adsorption layer of adsorbate on

adsorbent.

$$A(g) + S \xrightleftharpoons{adsorption} AS \qquad\qquad (6)$$
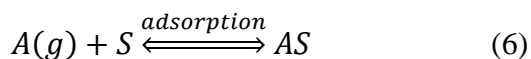
[A] = *P*= Pressure of gas; *[S]* = θ_V= concentration of available site;

[AS] = θ_1= concentration of sites occupied by first layer

Equilibrium constant for first layer $K_1 = \dfrac{[AS]}{[A][S]} = \dfrac{\theta_1}{(\theta_V)(P)}$ $\hspace{2cm}$ (7)

For n^{th} layer: $A(g) + A_{n-1}S \Longleftrightarrow A_n S$ $\hspace{2cm}$ (8)
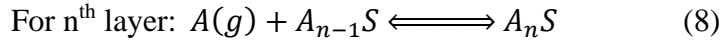
Equilibrium constant for n^{th} layer $K_n = \dfrac{\theta_n}{(\theta_{n-1})(P)}$ $\hspace{2cm}$ (9)

Using above, the linear form of BET equation is

$$\frac{1}{V_m\left[\frac{P}{P_o}-1\right]} = \frac{1}{V_m C} + \frac{C-1}{V_m C}\left(\frac{P}{P_o}\right) \hspace{2cm} (10)$$

Where P and P_o are the adsorbate equilibrium and saturation pressures, respectively, C is a BET

constant, V is quantity of the adsorbed gas, and V_m is the quantity of adsorbed gas by monolayer.

By plotting $\dfrac{1}{V_m\left[\frac{P}{P_o}-1\right]}$ against $\left(\dfrac{P}{P_o}\right)$, the values of slope s and intercept i can be calculated as

Slope $s = \dfrac{C-1}{V_m C}$ and intercept $i = \dfrac{1}{V_m C}$

According to the BET theory, the parameter C is exponentially related to the energy of

monolayer adsorption. The general consensus today is that the value of C actually provides a

helpful indication of the isotherm's shape within the BET range.

If the value of C is equal to or greater than approximately 80, the knee of the isotherm exhibits a

sharp characteristic.

When the value of C is low (less than approximately 50), there exists a significant overlap between monolayer and multilayer adsorption, leading to uncertainties in the accurate interpretation of V_m.

When the value of C is less than 2, the isotherm can be classified as either Type III or Type V. In such cases, the BET method cannot be used.

A high value of C (say, >150) is generally associated with either adsorption on high-energy surface sites or the filling of narrow micropores.[38]

Application of BET Equation

     I.   Specific monolayer capacity n_m and value of C

$$n_m = \frac{1}{s+i} \qquad (11)$$

$$C = \frac{s}{i} + 1 \qquad (12)$$

Furthermore, two conditions must be fulfilled for the satisfaction of this criterion of microporous surface area measurement:

(i) $\frac{1}{V_m\left[\frac{P}{P_0}-1\right]}$ value should increase with increasing $\left(\frac{P}{P_0}\right)$, and (ii) y intercept in the linear region of the graph must be > 0 to have a meaningful value of C.

     II.   Specific surface area

$$S_{BET} = \frac{n_m N A_x}{w} \qquad (13)$$

Where N is Avogadro's number, A_x is the cross-sectional area of the adsorbed gas molecule and w is mass of adsorbent. The accepted cross-sectional area of a nitrogen (N_2) molecule used in the calculation of BET surface area is 0.162 nm^2. This standardized value enables researchers from various laboratories to compare materials consistently.

3.3.3 The extended BET (Brunauer, Emmett and Teller) Model

The conventional BET method cannot be used to determine the specific surface area within the relative pressure range of 0.05 to 0.3 for microporous adsorbents with pore diameters below 2nm (20 Å).[56]

The prevalence of microporous adsorbents is primarily observed in the context of Type I isotherms. In this scenario, the micropores within the adsorbent material become completely occupied at extremely low pressures, reaching saturation prior to a relative pressure of 0.05. Consequently, this leads to a negative value for the BET constant C, rendering the application of standard BET calculations unfeasible.

In order to determine the specific surface area, it is necessary to employ additional consistency theory to identify the appropriate relative pressure range where the equation can be effectively applied and yield a positive value for BET constant C.

The Quantachrome Nova 2000e, a BET surface area and pore size analyzer, was employed to ascertain the adsorption isotherm. A total of 100 adsorption and desorption events can be graphed in a nitrogen bath at a temperature of 77 K. The pressure measurement accuracy is 0.1%. It is capable of measuring specific surface area greater than 0.01 m^2/g.

Method of using the first consistency theory to determine the microporous adsorbent's specific surface area.

    I.   Collect an additional ten or more data points within the relative pressure range of 0.05 to 0.5 using the standard BET experiment. The higher the number of points acquired, the more favorable the outcome.

    II.   A graph is to be plotted with $V_m(P^o - P)$ on y-axis and P/P^o on x axis. The locations of the plot's maxima should be noted.

    III.   The specific surface area can be calculated within the relative pressure range that extends from the lowest relative pressure to the point of maxima.

    IV.   Plot a straight line using a minimum of three data points from the aforementioned range (or more is preferable) and determine the maximum value of correlation coefficient R^2 derived from the combination of the data points.

    V.   Determine the value of the BET constant C, which must be positive, using the equation of the best-fitting straight line. Once a positive value of C is obtained, the calculated specific surface area within the specified range can be deemed acceptable.

This procedure is based on the following main criteria: (a) the quantity C should be positive (i.e., a negative intercept on the ordinate of the BET plot is the first indication that one is outside the appropriate range); (b) application of the BET equation should be restricted to the range where the term $nm(1 - p/p^o)$ continuously increases with p/p^o; (c) the p/p^o value corresponding to n_m should be within the selected BET range.[38]

3.3.4 The Freundlich Model (Two parameter model)

The reversible and non-ideal adsorption process is described by the Freundlich adsorption isotherm model. It can be applied to multilayer adsorption, unlike the Langmuir isotherm model, which is limited to monolayer formation. Adsorption heat and affinities do not have to be evenly distributed across the heterogeneous surface in this isotherm model.[57]

The equation of Freundlich isotherm model is an empirical equation. It was originally obtained by assuming heterogeneity of the surface in which the energy of adsorption is distributed, and topography of the surface is patch wise.

$$q_i^* = \frac{q_{i,max}(K_i P)^{1/n_i}}{1 + (K_i P)^{1/n_i}} \qquad (14)$$

Where q_i^* is the amount of the adsorbed phase of component i, $q_{i,max}$ is the maximum adsorbed amount of component i and n_i represents the adsorbent heterogeneity.

It is relevant for systems characterized by heterogeneous surfaces in the gas phase. The isotherm exhibits inadequate adherence to Henry's law at low pressure, resulting in a limited pressure range. When the pressure reaches a certain threshold, it does not possess a finite boundary. Therefore, it can be concluded that this adsorption isotherm model is not applicable to a wide range of adsorption data.[34,58]

3.3.5 The Toth Model (Three parameter model)

Designed to minimize the discrepancy between the experimental and predicted values, this isotherm model is an empirically modified version of the Langmuir equation. It is mostly used to describe heterogeneous adsorption systems that can handle both low and high concentrations of

adsorbate. The underlying assumption of this isotherm model is that there exists an asymmetrical quasi-Gaussian distribution of energy, wherein the majority of sites exhibit lower energy of adsorption compared to the mean value or the peak.[59]

At low concentrations, the Toth equation reduces to Henry's law; at high concentrations, the Langmuir isotherm model approaches a finite capacity more quickly.

Typically, the adsorption of vapors of organic compounds and other gases are described using this isotherm model.[36]

3.4 Adsorption equilibrium model for CO_2 capture by adsorbents

The Langmuir model postulates that adsorption takes place on a surface that is uniform in nature, having a limited quantity of identical sites. In contrast, the Freundlich model posits that adsorption happens on a surface that is diverse in nature, characterized by a range of site energies. The Toth model is a theoretical framework that integrates the Langmuir and Freundlich models, incorporating considerations for surface heterogeneity and the limited availability of adsorption sites.

3.4.1 Activated carbon

In the context of CO_2 adsorption from biogas, a study[60] compared the performance of Langmuir, Freundlich, and Toth models for describing the adsorption of CO2 onto activated carbon derived from coconut shells. The study found that the Toth model provided the best fit to the experimental data, followed by the Langmuir and Freundlich models. The authors attributed this to the fact that the Toth model takes into account both the heterogeneity of the surface and the finite number of sites, which are important factors in the adsorption of CO2 from biogas.

3.4.2 Zeolite

In the context of CO_2 adsorption from biogas, a study[61] compared the performance of Langmuir, Freundlich, and Toth models for describing the adsorption of CO_2 onto zeolites. The study found that the Langmuir model provided the best fit to the experimental data, followed by the Toth and Freundlich models. The authors attributed this to the fact that the Langmuir model assumes a

homogeneous surface, which is more appropriate for zeolites than the Freundlich model, which assumes a heterogeneous surface. The authors also noted that the Toth model provided a good fit to the experimental data, but was less accurate than the Langmuir model.

3.4.3 Magnesium oxide MgO

Magnesium oxide (MgO) has been widely studied as a potential adsorbent for CO_2 adsorption from biogas. Among the three adsorption models mentioned, Langmuir model is the most suitable for MgO-based adsorbents. The Langmuir model assumes the adsorption of one molecule does not affect the adsorption of another molecule.[62]

3.4.4 Metal organic frameworks (MOFs)

Metal oxide frameworks (MOFs) have been identified as highly efficient adsorbents for CO_2 storage. The Langmuir model is the most suitable for MOF-based adsorbents. However, Langmuir model is not the only model that can be used to describe adsorption. Other models such as Freundlich and Toth models can also be used depending on the specific adsorption system and the adsorbent material. [63]

Thus, these isotherms provide a quantitative representation of the adsorption process, and the selection of the appropriate isotherm depends on the particular characteristics of the solid adsorbent as well as the nature of the CO_2 adsorption process.

Chapter 4

Textural characteristics of adsorbents

4.1 Introduction to physical characteristics of adsorbents

The textural properties of the adsorbent, such as surface area, pore volume, and pore size, are crucial factors in gas adsorptive separation processes using microporous adsorbents. When the pore size of a material falls within the range of kinetic diameters of two gas molecules, namely carbon dioxide (CO_2) with a diameter of 3.3Å and methane (CH_4) with a diameter of 3.8Å, it becomes possible to separate these gases through a phenomenon known as molecular sieving effect or steric effect. When the pores possess appropriate dimensions, only the smaller molecule (CO_2) is capable of diffusing into the pores, while the larger molecule (CH_4) is completely precluded. If the pore size is slightly larger than the kinetic diameter of the larger molecule (CH_4), one can separate the two gases by a kinetic separation, which is achieved by the difference in the diffusion rates. It is observed that the larger molecule, namely CH_4, exhibits a slower rate of diffusion in comparison to the smaller molecule, CO_2. In cases where the pore size is sufficiently large to allow for the easy diffusion of both molecules into the pores, the separation of the two molecules can be achieved through differences in their equilibrium adsorption. This principle is commonly employed in a significant majority of adsorptive separation techniques. The pore size and thus surface area may influence how much is adsorbed, even in separation procedures that rely on variations in equilibrium adsorption.[64,65]

4.2 Evaluation of surface area & pore volume of adsorbents

4.2.1 Zeolite 13X isotherm

Fig. 1 shows adsorption-desorption isotherm for zeolite 13X measured at 77 K. It exhibits

characteristics consistent with the IUPAC Type I isotherm, wherein a pronounced rise in

adsorbed gas volume occurs at very low pressures, followed by a subsequent rise to a stable

plateau as pressure increases. Furthermore, the presence of hysteresis gives confirmation of the

lack of mesoporosity. Therefore, zeolite 13X can be classified as a microporous adsorbent with a

pore radius of less than 20Å. The BET model, an extended version of the Langmuir isotherm, is

a suitable fit for the Type I isotherm. However, as can be seen from the graph, using the

traditional BET equation—which yields a positive BET constant C in the range of 0.05 to 0.30

relative pressure—to compute a specific surface area is challenging. The graph reaches a

horizontal plateau in the previously mentioned relative pressure range, signifying that micropores

have already filled within that range, which explains why. Therefore, it is necessary to

implement an additional step that expands the application of the BET by incorporating first

consistency theory.
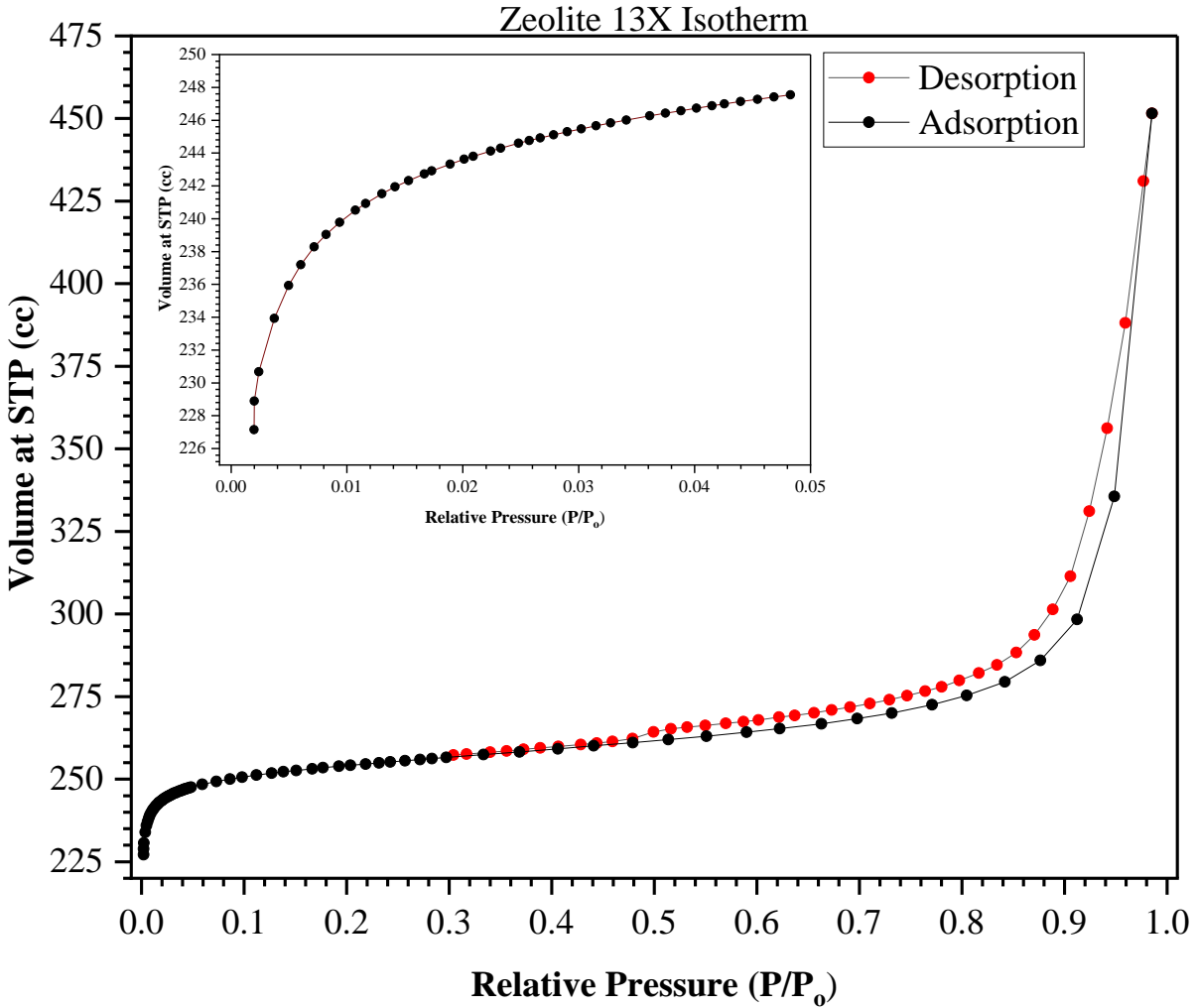
Figure 1. Adsorption-desorption isotherm of Zeolite13X at 77K in nitrogen gas

The first consistency theory in the range of 0.001 to 0.05, as shown in figure 1.1, satisfies both of its requirements by providing a positive value for C and a straight line with a positive slope as relative pressure is increased. For zeolite 13X, the specific surface area calculated using the aforementioned method is 492 m^2/g. The specific surface area falls within the range of 472 m^2/g to 591 m^2/g.[66–74]
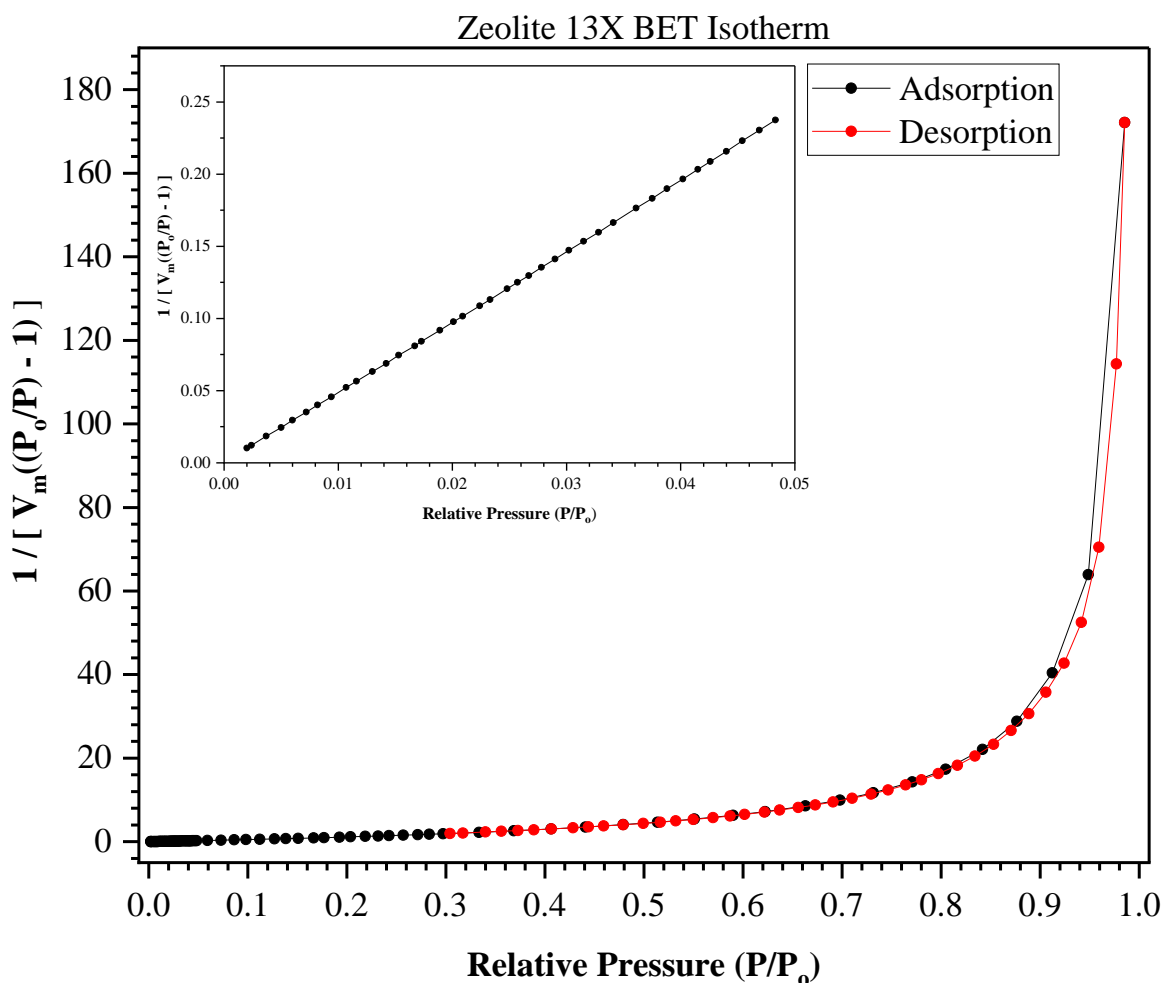
Figure 1.1 BET isotherm of Zeolite13X at 77K in nitrogen gas

The marginal variation in specific surface area may be ascribed to the hydrothermal treatment to synthesize zeolite from silica and alumina. To decrease the expense of synthetic zeolites, an assortment of silica and alumina sources are utilized, including waste porcelain, kaolinite[66], bentonite[67], lithium slag[68], high silicon fly ash[69], paper sludge[70,71], oil shale ash[72], and coal fly ash.[73] For instance, 13X derived from natural kaolin exhibits a high surface area of 591 m^2/g, whereas that produced from feldspath demonstrates a low surface area of 472 m^2/g.[74]

The widely utilized method for characterizing the pore size distribution in the mesoporous and a portion of the macroporous range is the classical pore size BJH model. This model incorporates

corrections for multilayer adsorption and is based on the Kelvin equation.[75,76] The primary

utilization of the HK model, originally formulated to describe the presence of slit-shaped pores

frequently found in carbon materials & zeolites, is to determine the pore sizes of materials that are

predominantly characterized by microporosity.[77] The DFT model is a comprehensive quantum

mechanical framework employed for the analysis of the textural properties of porous materials that

encompass pores of different dimensions, with respect to the equilibrium density profile of a fluid

in contact with a surface.[78]

The HK model is considered to be more favorable for analyzing the distribution of pore volumes,

as it exclusively generates differential pore volumes within the microporous range. The

aforementioned advantage may stem from the underlying assumption that the zeolite possesses a

morphology characterized by a slit shape. However, it can be inferred that this particular model is

not suitable for the comprehensive analysis of materials exhibiting a wide spectrum of porosity. It

is apparent that the BJH and DFT models exhibit a significantly wider spectrum of pore sizes

compared to the HK model, thereby providing a more comprehensive analysis of mesoporous

materials.[76]

The differential surface area distributions, as determined by the BJH and DFT models, have been

found to be unsatisfactory in their outcomes for microporous materials as reported by previous

researchers.

In the present case, the pore size distribution for zeolite 13X, as determined by the HK model, was

found to be 0.270 cc/g. It is consistent with the pore size discovered by other comparable

techniques, such as the t-plot method(0.240 cc/g)[74], DR method (0.298 cc/g)[79], and HK method

(0.250 cc/g)[65] for zeolite 13X.

Fig. 1.2s shows adsorption-desorption BET isotherm for natural zeolite clinoptilolite. The present study employs the BET) first consistency theory to determine the specific surface area of natural zeolite. As observed, the relative pressure in this particular instance is comparatively lower than that of Zeolite 13x, ranging from 0.05 to 0.12. These values satisfy the conditions outlined in the first consistency theory, and also yielding an r-square value of 0.9792.
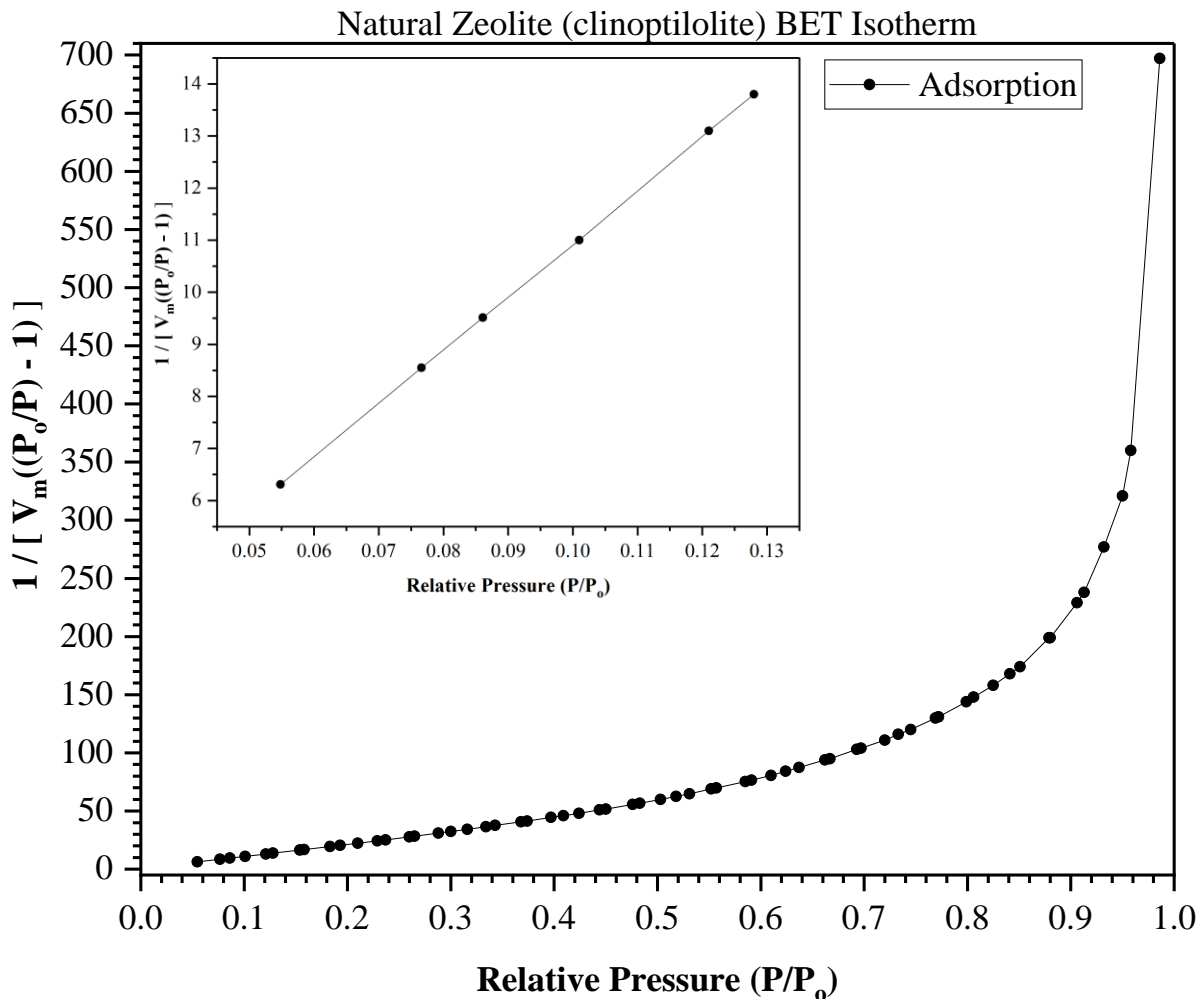
Figure 1.2 BET isotherm of natural zeolite (clinoptilolite) at 77K in nitrogen gas

The specific surface area achieved is 42 m^2/g, which is nearly one-tenth of the value observed for zeolite 13X. The specific surface area measured in this study falls within the reported range of 25 m^2/g to 49 m^2/g observed by other researchers.[80,81] The source from which natural zeolite is

produced can be used to explain this slight variation in surface area. As an illustration, it can be observed that a zeolite originating from Texas, USA exhibits a relatively lower specific surface area of approximately 25 m^2/g, whereas another zeolite sourced from Idaho, USA demonstrates a comparatively higher specific surface area of approximately 42 m^2/g.[80]

The micropore volume of the natural zeolite was determined to be 0.0137 cc/g and 0.01044 cc/g using the HK and SF methods, respectively. The micropore volume reported by other authors, ranging from 0.025 cc/g to 0.043 cc/g, is higher than the value mentioned.[80–82] The observed discrepancy can be ascribed to variations in the methodology employed for calculating micropore volume, as well as the presence of small values, which amplifies the potential for error. However, according to researchers' reports, it is nearly within the range.

4.2.2 Activated carbon isotherm

Activated carbon is a type of porous adsorbent that contains pores of various sizes. These pores can be classified as micropores (less than 2.0nm in width), mesopores (2-50 nm in width), and macropores (greater than 50 nm in width). For the majority of activated carbons, the adsorption isotherms closely resemble type I, as the majority of the adsorbed volume is found within micropores. The presence of diverse porosity complicates the analysis of adsorption isotherms.[83] The type 1 isotherm is shown in Figure 2 when the relative pressure is low, while the type 5 isotherm is shown when the relative pressure is higher. The presence of mesopores in phase changes, such as pore condensation, is indicated by this type of pore. At this point, there is only one point of inflection.
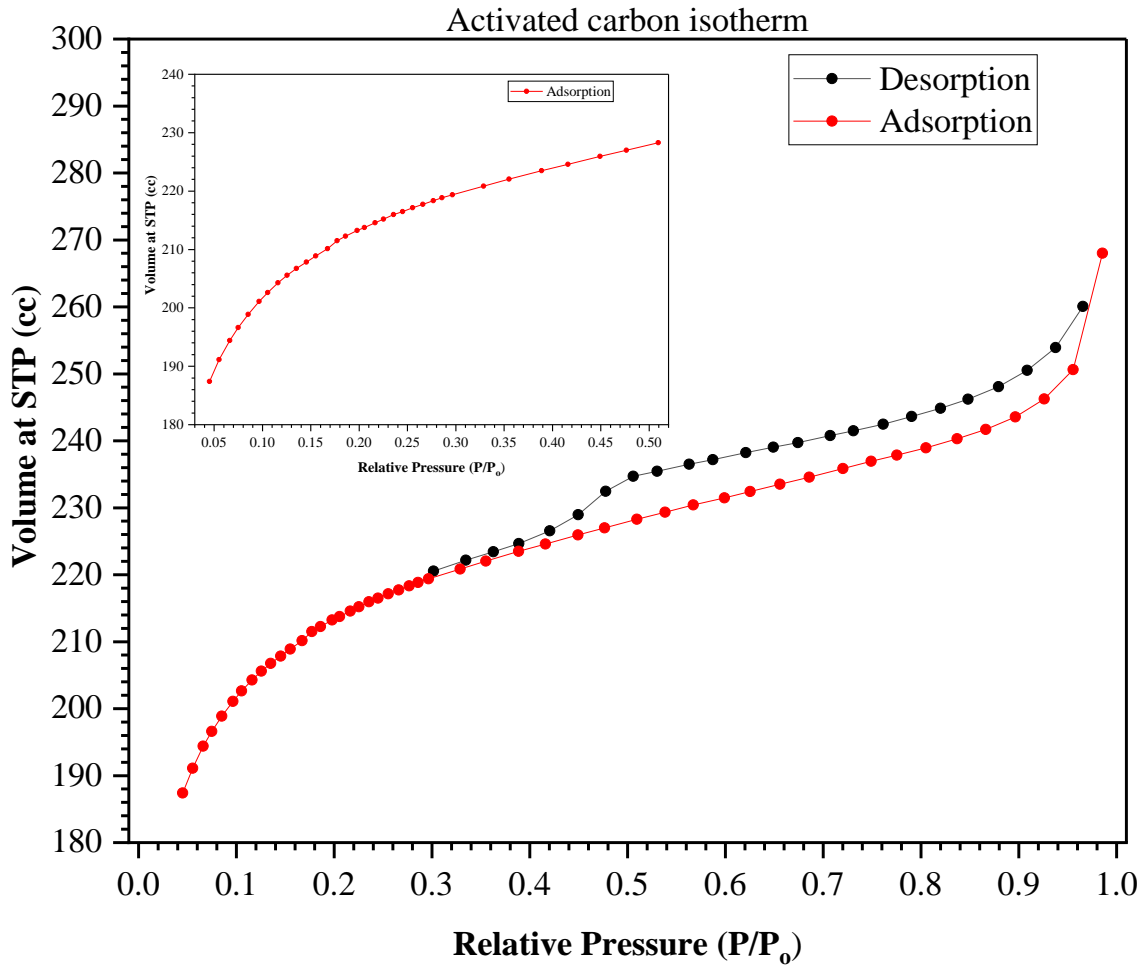
Figure 2. Activated carbon isotherm

The specific surface area of activated carbon in line with first consistency theory was found to be 8.9e+01 m²/g as shown from figure 2.1. While micropore volume using t method, DR method and SF method is calculated as 3.5e-01 cc/g.
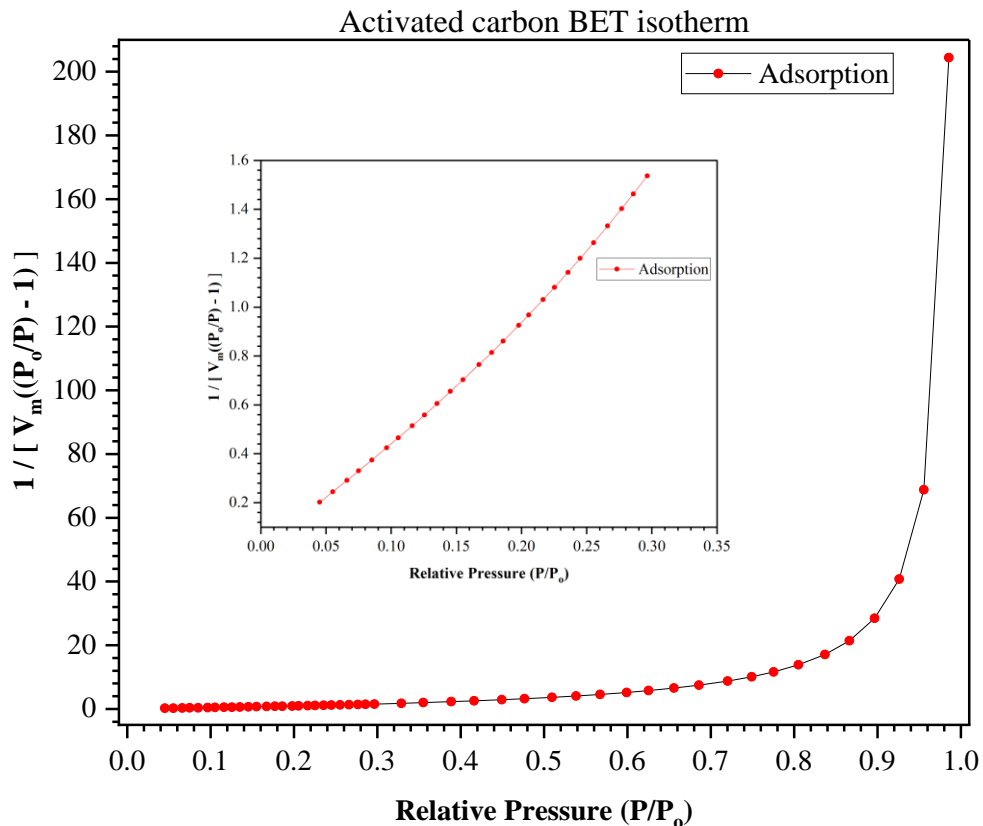
Figure 2.1 BET isotherm for activated isotherm

4.2.3 Magnesium oxide isotherm

The isotherm of magnesium oxide exhibits similarities to that of zeolite 13x, although it adsorbs a significantly smaller volume of gas at equivalent relative pressures as shown in figure 3. The microporous surface area is determined within the relative pressure range of 0.005 to 0.04, as per the "first consistency theory" mentioned earlier. The hysteresis loop confirms the lack of mesopores.
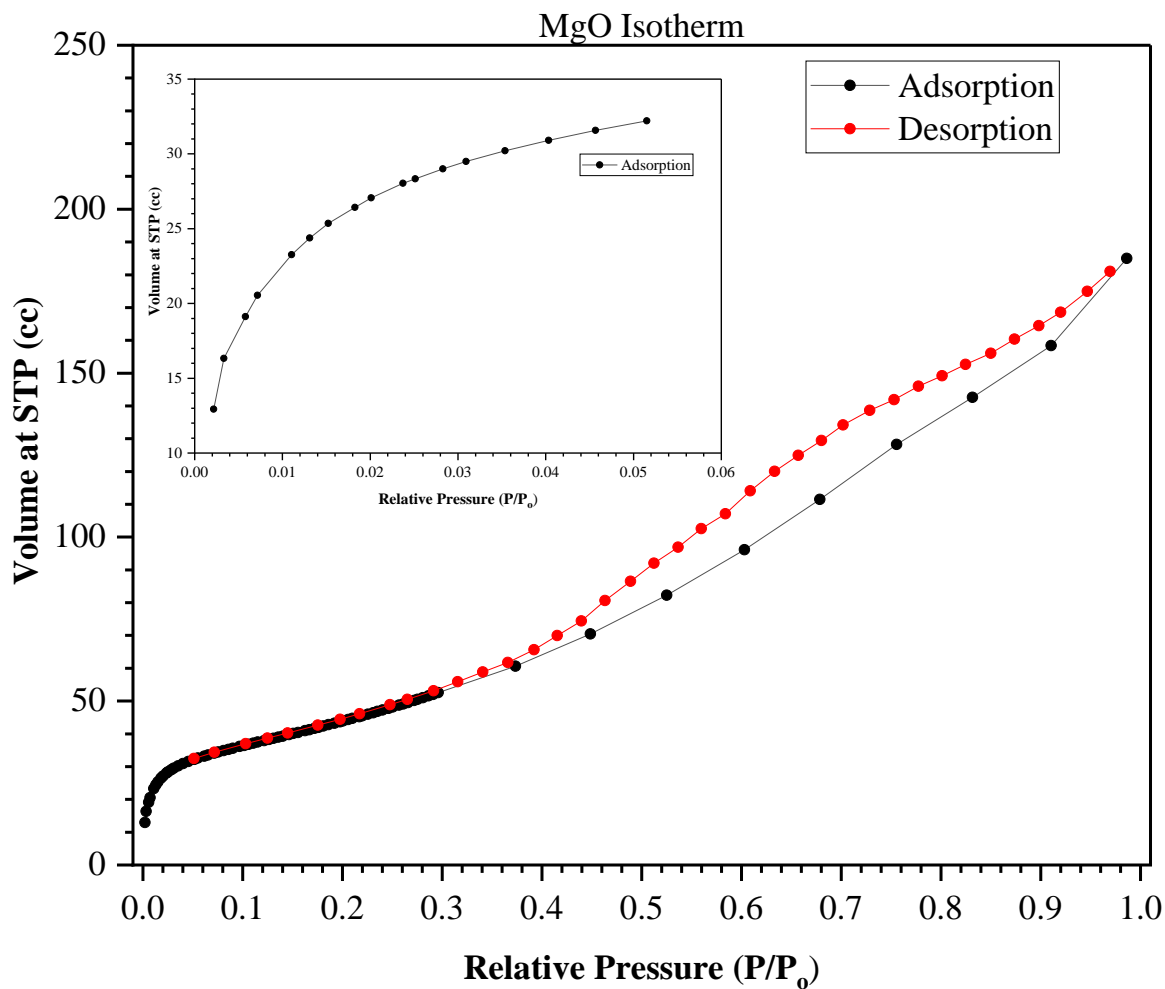
Figure 3: Magnesium oxide isotherm at 77K

According to the data presented in Figure 3.1, the specific surface area of microporous magnesium oxide is determined to be 5.9e+01 m²/g, which is relatively lower than the surface area of the adsorbents mentioned earlier. The micropore volume, determined using the DR and HK methods, is measured to be 1.113e-01 cc/g.
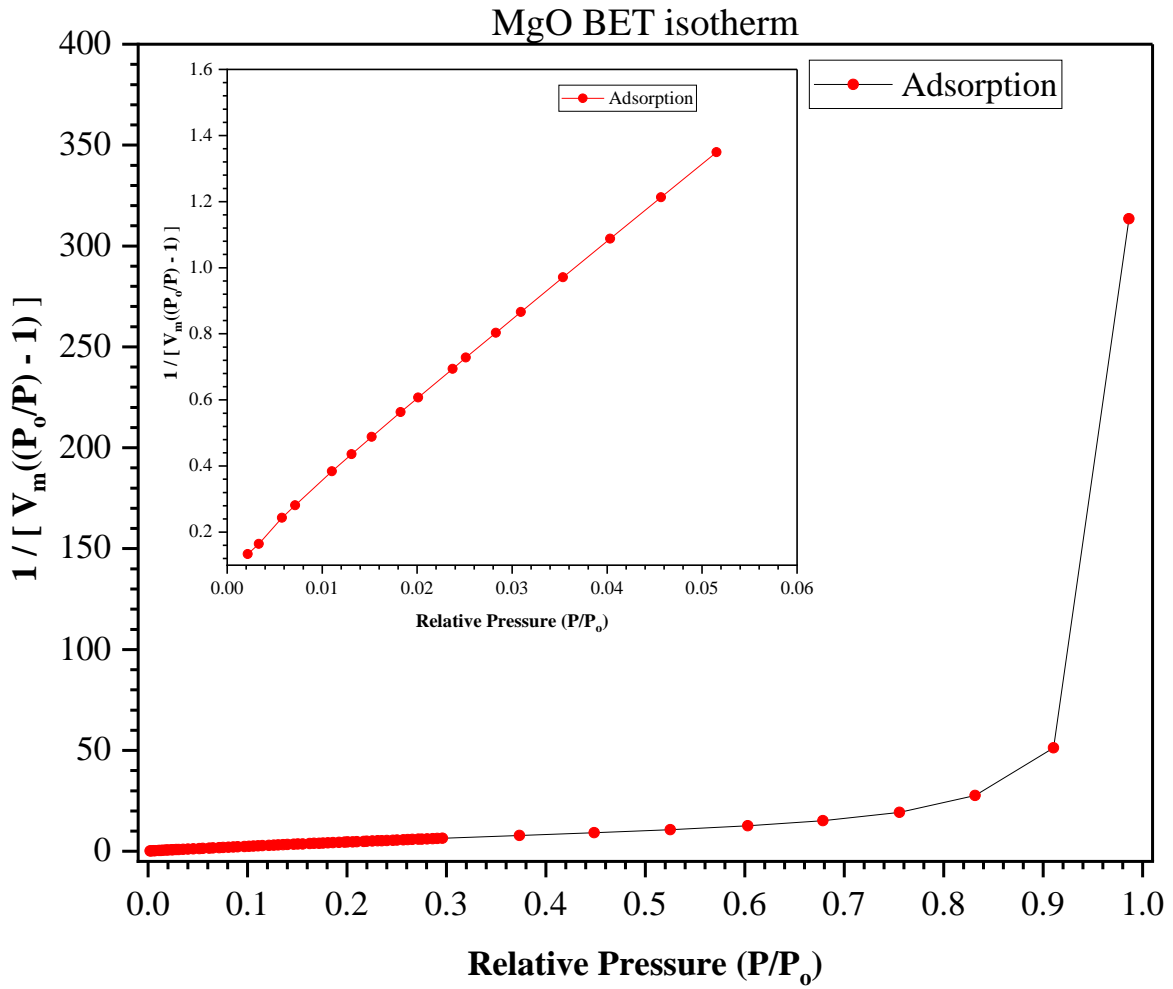
Figure 3.1 BET isotherm for magnesium oxide at 77K

Chapter 5

Experimental setup

5.1 Experimental methodology for adsorption using Thermogravimetric analysis TGA

The adsorption capacity, defined as the quantity of gas adsorbed under the specified feed conditions, serves as a common metric employed by material researchers to showcase the potential of novel materials and to facilitate comparisons with existing commercial adsorbents.[84] One of the methods for determining the adsorption capacity of an adsorbent can be achieved through the analysis of breakthrough curves. Breakthrough curves represent the variation over time of the concentration of the adsorbate in the biogas. The breakthrough point refers to the specific moment when the concentration of the adsorbate in the biogas begins to exhibit an increase that is discussed later in detail. The quantity of adsorbate that has been adsorbed by the adsorbent until the point of breakthrough can be determined through calculation or area under the breakthrough curve. The determination of the adsorption capacity of the adsorbent can be achieved by calculating the ratio of the mass of the adsorbate adsorbed to the mass of the adsorbent employed. The quantification of the adsorbent's adsorption capacity is typically denoted in terms of the mass of adsorbate per unit mass of adsorbent, commonly expressed as mg/g or g/kg.[85,86] The practice of determining adsorption capacity from a breakthrough curve is commonly employed; however, it is preferred for adsorbents that are obtainable in grams and kilograms quantities. When conducting a comparison of novel adsorbents synthesized in

milligrams, an alternative approach to determine their adsorption capacity is through the Thermogravimetric Analysis (TGA), which involves the use of milligrams quantities of the adsorbents. The experiment employed instruments Q5500 Thermal Gravimetric Analyzers (TGA) with a weighing accuracy of -0.1%, weighing precision of 0.01%, sensitivity less than 0.1 µg, and furnace heating through infrared technology, capable of covering a temperature range from ambient to 1200 degrees Celsius.

By using TGA to measure weight increases and decreases during the adsorption processes, the adsorbent's CO_2 adsorption capacity was evaluated. To remove moisture from the specimen, the temperature was first raised from 25 °C to 120 °C at a rate of 10 °C/min for 60 minutes while the specimen was submerged in pure N_2 (99.995%). The temperature was then lowered to 25 °C and maintained for 60 minutes to allow for CO_2 adsorption, but this time under pure CO2 (99.9%). In order to facilitate desorption, the temperature was finally raised to 120 °C and the gas flow was switched from CO_2 to N_2. Calculating CO_2 adsorption capacity (mg-CO_2/g-sorbent) involved applying TGA to measure the sample's weight change during the adsorption and desorption processes.[87]

5.2 Design of experiment for fixed bed column adsorption

The experimental design is depicted in Figure 4. Stainless steel is used for all pipe connections. CO_2 and N_2 are passed through respective mass flow controllers as shown. The maximum flow rates of the mass flow controllers, which are purchased from Alicat, are 50 sccm and 100 sccm. Mass flow controllers were calibrated using a gas bubble flow meter. Before being injected from below into the adsorption column, N_2 and CO_2 are mixed 50:50 in a gas mixer. The purpose of this biogas simulation is to better understand how an adsorbent captures CO_2 gas molecules. After the gas mixer leaves the column, the simulated biogas is diluted using a Testo gas analyzer, which is used to measure the CO_2 concentration. The experiment used a Testo 350 gas analyzer, which measured CO_2 using infrared radiation (IR) with a 0.2 volume% accuracy and a 0.01 volume% resolution. The analyzer's pump requires a minimum of one liter of input per minute, so the gas mixture is diluted by ambient air by a factor of one. Every value for the experiment is recorded by the analyzer at a rate of one dataset per second. Made of stainless steel, the adsorption column has a 90 cm^3 capacity. A pressure transducer and a k type thermocouple are connected at the top of the column to measure the pressure and temperature, respectively, in the adsorbent-filled column. Depending on the procedure used, the outlet gas can be moved to a vacuum or a gas analyzer using a needle valve. In addition, heat tape with a maximum temperature of 200 °C is wrapped around the column in order to conduct temperature swing adsorption. Data values from the data acquisition system DAQ are used to measure the mass flow rate from MFCs, the temperature from a K thermocouple, and the pressure inside a column from pressure transducers. MicroDAQ is the source of the DAQ model number USB-2416-4AO, which has a sampling rate of 1 kS/s. All inputs are gathered at one dataset per second, up to three decimal places, using compatible software.
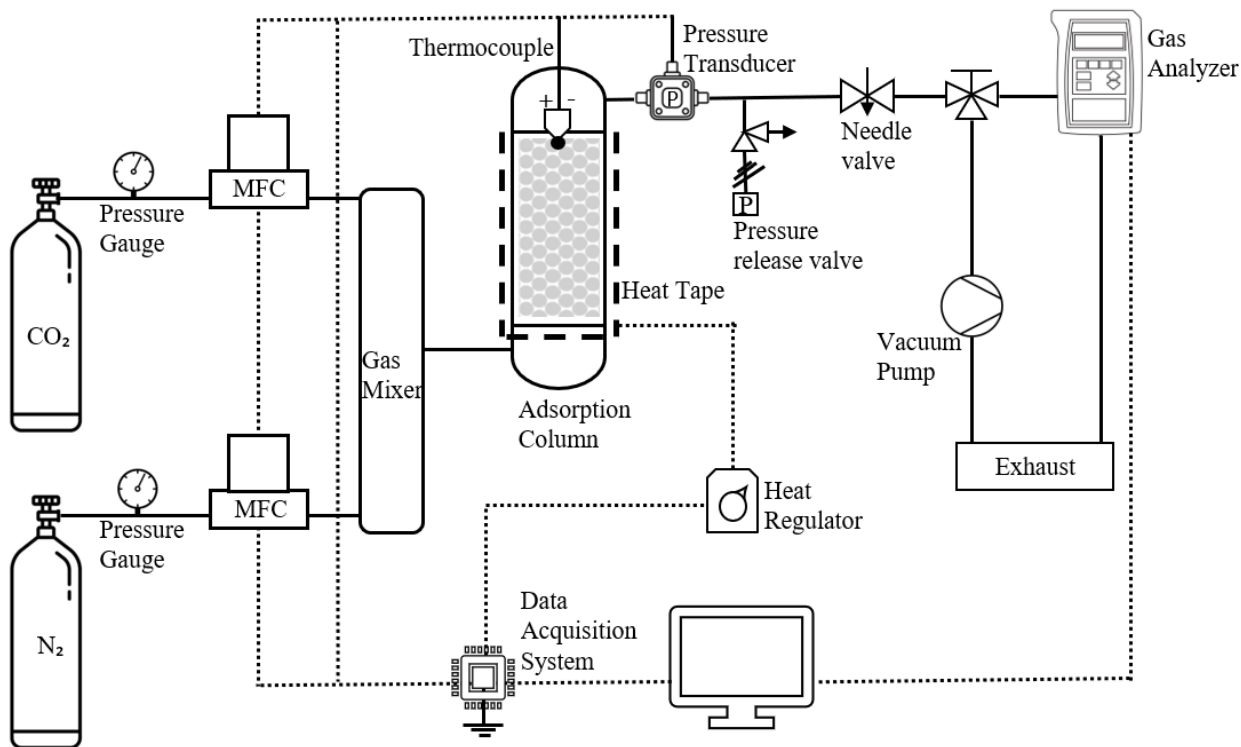
Figure 4 Experimental setup layout for PVSA and TSA.

Figure 4.1 shows the actual experimental setup, with the testo gas analyzer at right and the data acquisition system connected to the computer at left. Figure 4.2 shows the adsorption column wrapped up in heat tape. As can be seen, two MFCs are positioned on a aluminum bench and are supplied with gas via fume hood ducts.

Figure 4.1 Actual experimental setup

Figure 4.2: Actual adsorption column

5.2.1 Vacuum pressure swing adsorption

In the experimental setup, the needle valve is initially maintained in an open position in order to establish a pressure within the column that is equivalent to atmospheric pressure. The adsorbent-filled column is supplied with 50 sccm of nitrogen and carbon dioxide each, using mass flow controllers. In this stage of the feeding process, the mixture continues to flow until the detection of a CO_2 at 50 sccm at the outlet, commonly referred to as the exhaustion point. At that moment, the adsorbent is regarded as being completely saturated. The gas flow from the inlet is stopped and a vacuum is applied at the outlet by connecting it to the needle valve for the blowdown process. A vacuum pressure of -11 PSIG is employed from the upper part of the column in order to remove adsorbed CO_2 from the adsorbent material. After the majority of the captured CO_2 has been eliminated, the final stage involves a process known as purging. During the process, a flow rate of 100 sccm of N_2 gas is employed to flush the column. This serves two purposes: restoring the pressure within the column to atmospheric levels and eliminating any residual trapped CO_2 in the adsorbents, if present. The aforementioned sequence of feed, subsequently blowdown, and finally purging is iterated on the same column under the same conditions in order to evaluate the regeneration of the adsorbent through the utilization of the (VPSA) process.

5.2.2 Temperature swing adsorption

During the experimental procedure, the heat tape is heated to a temperature of 120 °C. Additionally, the adsorbent material was heated prior to the feed step. The process being referred to is commonly known as the activation of the adsorbent. During the feeding step, a mixture consisting of N_2 at 50 sccm and CO_2 at 50 sccm with the same composition as PSA is supplied at atmospheric pressure and room temperature. After reaching the breakthrough point, the column is subjected to heating once more, raising the temperature to 120 °C. Simultaneously, a supply of

N_2 gas is introduced at a flow rate of 100 sccm. In the TSA process, the use of vacuum is not employed during the blowdown step. The process is continued until a significant portion of CO_2 that has been captured by the adsorbent is removed by flushing it out using nitrogen gas at a temperature of 120 °C. This process is subsequently replicated to determine the regeneration of the adsorbent under the same circumstances.

As part of an investigation into the combination of vacuum pressure and temperature swing adsorption, 120 °C is used to activate the adsorbent. Under the same conditions—room temperature and atmospheric pressure—the adsorption takes place in the column. A blowdown procedure is carried out at a temperature of 120 °C and a vacuum of -11 PSIG until CO_2 is desorbed. At room temperature, 100 sccm of nitrogen is employed to purge the column. To compare the regeneration of the adsorbent, the cycle is repeated.

Chapter 6

Breakthrough curve for CO_2 and N_2 adsorption/desorption process

6.1 Introduction to breakthrough curve

The main methods by which the contact between the adsorbate and the adsorbent occurs in the adsorption system are batch, continuous moving bed, continuous fixed bed (up flow or downflow), continuous fluidize bed, and pulsed bed. In the batch sorption process, adsorbate and adsorbent are mixed in a diluted solution at a constant volume. Adsorbent is fixed in the fixed bed sorption process while adsorbate is continuously flowed through it. Continuous bed sorption occurs when both the adsorbate and the adsorbent are in constant motion. Adsorbate is in contact with a fluidized bed of adsorbent with sufficient or insufficient flow in continuous fluidized bed sorption. Finally, in pulsed bed sorption, the adsorbate is contacted with the same adsorbent in the bed until the desired results are not obtained.[88–91] Because fixed bed sorption is simpler and more inexpensive to use, and is widely used in industrial processes to remove contamination, this study focuses solely on the fixed bed adsorption process.

6.2 Terminologies and graphical interpretation of breakthrough curve

The relationship between the nature of breakthrough curves and fixed-bed adsorption could be expressed as effectively using mass transfer zone (MTZ) or primary sorption zone (PSZ).[88] As shown in Figure 5, when the feed gas mixture is introduced through the column's inlet, the lower layers of the fresh adsorbent adsorb the adsorbate most quickly and efficiently in the early stages of the process. This is because there is no adsorbate (in this case, CO_2) run off from the adsorbent at the first stage, and there is a greater amount of adsorbent and less adsorbate available at these lower layers, allowing adsorbate to be easily escaped in the upper strata of the bed. Thus, the MTZ, or primary adsorption zone, is reached close to the bottom or start of the column. The ratio of the starting concentration (C/C_o) is now zero since the concentration of the adsorbate (C) is zero. After that, as adsorbate is fed into the column, the lower layer of the adsorbent gradually becomes saturated and loses some of its effectiveness. As a result, the main sorption zone ascends to the section of the adsorbent in the column that is fresher or has not yet been adsorbed. Additionally, as this zone moves, there is a tendency for an increasing amount of adsorbate to exit the effluent at points. In contrast to the feed gas's linear velocity, the movement of this zone primarily increases with increasing initial concentration. Adsorption stops when the column is fully saturated or exhausted, which happens after a certain amount of time (C_s). The ratio of C/C_o then becomes near to one.
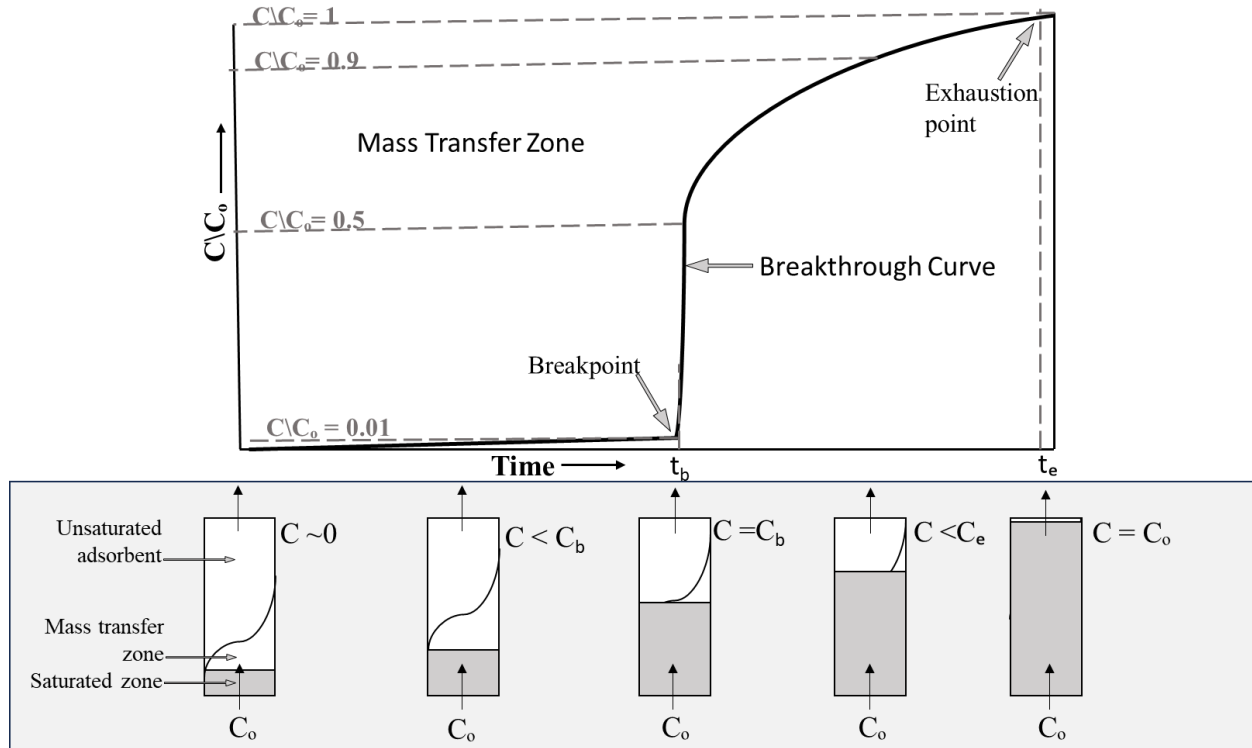
Figure 5. Schematic representation of adsorption column and breakthrough curve characteristics

An ideal breakthrough curve, as shown in figure 6, has an exhaustion point C_x at the very near CO_2 concentration of the adsorbate and a breakthrough point C_b when CO_2 is first detected, or when the ratio of C/C_o is around 0.01. The volumes of CO_2 in this case are V_b and V_x, which stand for the concentrations of the break point C_b and exhaustion point C_x, respectively. The area of the adsorbate concentration between the exhaustion points C_x and breakthrough point concentration C_b is known as the primary sorption zone (PSZ). Certain critical parameters, such as the total time required for the primary sorption zone to establish itself (t_x), the time it takes the exchange zone to move the length of its own height up or down the column (t_δ), the rate at which the exchange zone moves up or down through the bed (U_z), the fraction of adsorbate present in the adsorption zone (F), and the percentage of the total column saturated at breakthrough, are

calculated using basic equations if PSZ is assumed to have a constant length or depth (δ). These factors are essential for designing columns.[88,92,93]
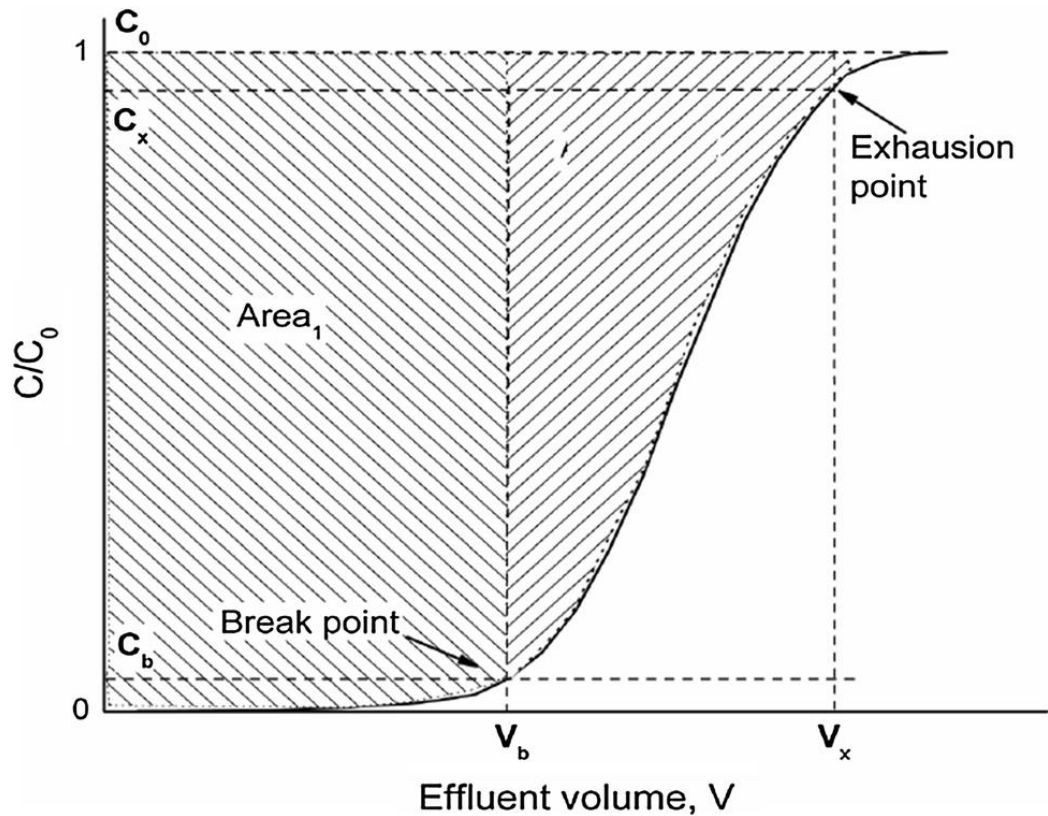
Figure 6: Ideal breakthrough curve[88]

It is possible to assess the effects of different process parameters, including breakthrough and exhaust points, pH of the adsorbate, particle size of the adsorbent, bed height of the column, initial adsorbate concentration, and flow rate of the adsorbate in the column. When assessing an adsorbent's capacity in an ongoing process, whether on a pilot or industrial scale, all of these parameters are crucial. The most practical of these parameters are the initial adsorbate concentration, bed height, and flow rate because these have been the focus of most recent research and are used to remove a variety of pollutants using both natural and synthetic adsorbents. With an increase in the initial adsorbate concentration, breakthrough and exhaustion

49

points happen sooner. After that, as the inlet concentration increased, the breakpoint time decreased. Adsorption initially proceeded quickly due to the abundance of available empty sites. Subsequently, elevating the initial concentration of adsorbate leads to an increased driving force for overcoming mass-transfer resistance. These speeds up the exhaustion of the sites, consequently decreasing the volume of effluent treated.[94,95] The amount of adsorbate adsorbed onto unit bed height (the mass-transfer zone) increases with increasing flow rate, resulting in a faster saturation rate and an increase in the mass transfer rate.[96] Adsorbate has more time to come into contact with the adsorbent at a lower flow rate, which leads to a higher removal of adsorbate in the column.[97,98] As bed depth increases, breakthrough and exhaustion times decrease. Furthermore, it was found that as bed depth increased, so is the volume of adsorbate treated. This was explained by a rise in the surface area and quantity of binding sites that were open to adsorption. As the amount of adsorbent increased, so did the time it took for the adsorbate and adsorbent to interact.[99,100]

6.3 Breakthrough curve adsorption models

6.3.1 Brief overview of adsorption models

Several mathematical models have been developed to assess the efficiency and suitability of column models for large-scale operations. The Thomas, Adams and Bohart model, as well as the Yoon-Nelson model, are commonly used for the analysis of column behavior in adsorbent-adsorbate systems. There are several reasons why they can be used everywhere. For one reason, the fact that linearized forms of all three models are available makes it easy to fit data using linear regression. Another reason is that the Bohart-Adams and Thomas models are easy to use because they don't need a lot of information to work. For example, you don't need to know about the bed void fraction or the adsorbent density. At the very end of the scale, the Yoon-Nelson model doesn't even need flow rate or bed length. It doesn't need any of the usual system and operational variables.[101–103] Table 3 displays the information regarding the adsorption models and their corresponding parameters. The column adsorption model exhibits variability with respect to the increasing operation parameters.

Table 3: Fixed bed column breakthrough model and parameter variation as operating conditions increase[88,101,104,105]

Breakthrough adsorption model	Linear equation	Plot	Model para-meter	Operating Conditions		
				Initial conc.	Feed rate	Bed height
Adam and Bohart model	$ln(\frac{C}{C_o})] = K_{AB}C_o t - K_{AB}N_o(\frac{Z}{F})$	$ln[(\frac{C}{C_o})]$ vs time	K_{AB}	Increase	Increase	Decrease
			N_o	Decrease	Decrease	Increase
Thomas model	$ln[(\frac{C_o}{C}) - 1] = \frac{K_{TH}q_o m}{Q} - \frac{K_{TH}C_o V_{eff}}{Q}$	$ln[(\frac{C_o}{C}) - 1]$ vs time	K_{TH}	Decrease	Increase	Decrease
			q_o	Increase	Decrease	Increase

Yoon Nelson model	$\ln\left(\frac{C}{C_0-C}\right) = K_{YN}t - \tau K_{YN}$	$ln\left(\frac{C}{C_0-C}\right)$ vs time	K_{YN}	Increase	Increase	Decrease
			τ	Decrease	Decrease	Increase

Following the acquisition of breakthrough curves, the correlation coefficient value r^2 for the aforementioned models is computed from the straight-line graphs. The coefficient of determination is useful because it indicates the proportion of one variable's variance (fluctuation) that is predictable from the other variables. This number is significant for all adsorption isotherms. A coefficient value that approaches unity denotes the most suitable isotherm model for the adsorbate-adsorbent system.[106]

6.3.2 Bohart Adam model

The Adam–Bohart model is the equation for the relationship between C/C_o and time in a continuous system that scientists, specifically Bohart and Adams, studied. Fundamentally, gas–charcoal adsorption systems were used in novel research by Adam and Bohart, and their equation can subsequently be applied to other continuous adsorption systems. According to this model, the sorbing species' concentration and the adsorptive residual capacity determine the adsorption rate. Its function is to depict the preliminary segment of the breakthrough curve, which establishes a relationship between C/C_o and time. The model operates under the assumption that the adsorption process takes place in a well-mixed adsorber under consistent chemical and physical conditions. Additionally, it is assumed that the adsorption process is spontaneous and irreversible. The Langmuir isotherm, which describes adsorption onto a homogeneous surface, is an example of a linear isotherm that works well with it. More complicated isotherms, like the Freundlich isotherm, which characterizes heterogeneous adsorption surfaces, might be more difficult to predict with this method.[101,107]

6.3.3 Thomas model

This model was originally developed to describe liquid phase ion-exchange in fixed bed columns.[108] It is based on the assumption that equilibrium does not occur immediately in bed, and thus the rate of sorption is directly proportional to the fraction of sorption capacity that remains on the media. The relationship between bed depth and service time in terms of process concentrations and adsorption parameters provides the basis for this model. The surface reaction between adsorbate and the unused capacity of the adsorbent maintains the adsorption rate, according to this model. Instead of the bed height, the sorbent quantity is therefore preferred.[109] It works best for non-linear isotherms like the Freundlich isotherm, which describes heterogeneous adsorption surfaces. The model may not be suitable for linear isotherms like the Langmuir isotherm, which describes homogeneous surface adsorption. If Langmuir isotherm is followed and second-order reversible reaction kinetics are used, Thomas model fits well.

6.3.4 Yoon Nelson model

This model was developed to explain the innovative features of adsorption cartridges for respiratory protection.[110] It is based on the assumption that the rate at which the probability of sorption for each sorbate molecule goes down is related to the chance of sorbate sorption and sorbate breakthrough on the sorbent. During the adsorption process, the model takes into account both the external mass transfer resistance and the intraparticle diffusion resistance. The Yoon-Nelson model considers that the adsorption process follows the dual-porosity model, which says that the solid phase is split into two parts: an outer layer that moves and an inner layer that stays still. The model also considers that the adsorption kinetics are either first-order or pseudo-second-order. It works well with non-linear isotherms and can make more accurate predictions

for fixed-bed adsorption systems than models that look at mass transfer resistance from the

outside.[29,101,110]

Chapter 7

Results and observations

7.1 Zeolite 13X

7.1.1 Adsorption capacity by TGA

The TGA method can be used to determine the adsorption capacity, as shown in figure 7.

Adsorbent weight changes are proportional to the amount of carbon dioxide that is absorbed by

the adsorbent. Prior to introducing CO_2, the adsorbent was subjected to a temperature of 120

degrees Celsius for a duration of 60 minutes in the presence of nitrogen gas. This process aimed

to eliminate any moisture that may have been trapped. The same procedure was carried out for

other adsorbents. The adsorption capacity is 2.44 mmol of CO2 per gm adsorbent.
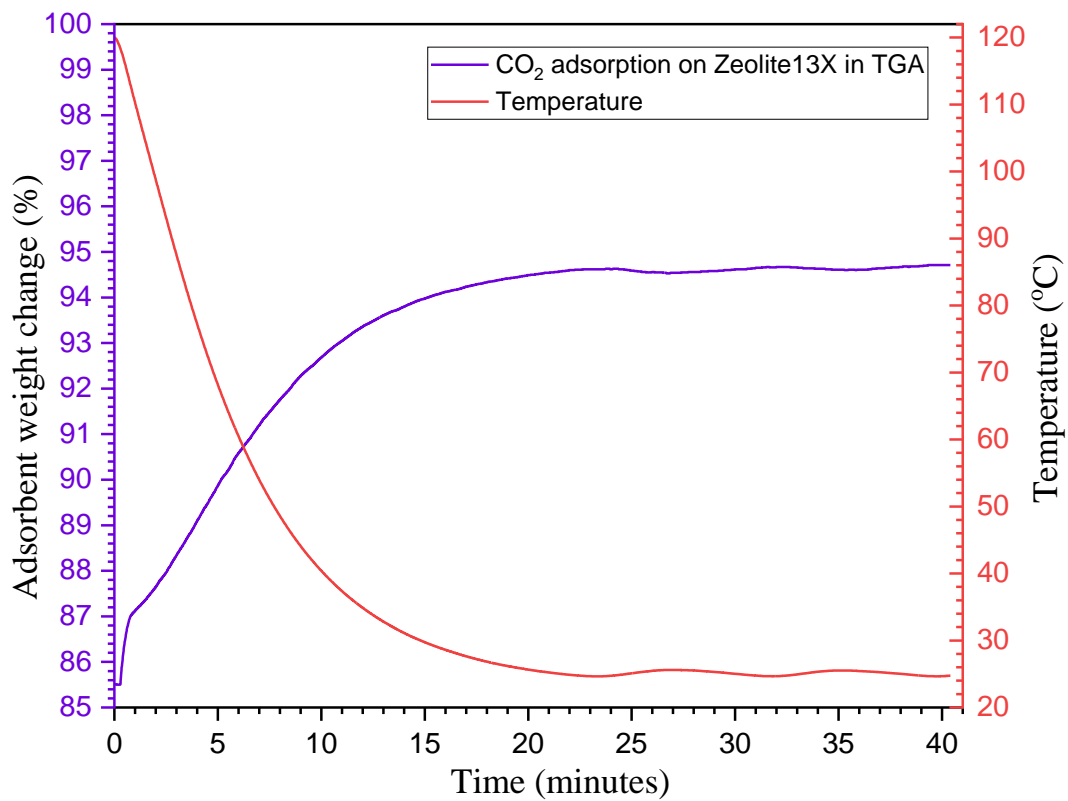
Figure 7: Breakthrough curve of zeolite 13X by TGA

7.1.2 Breakthrough curves by VPSA, TSA and combination
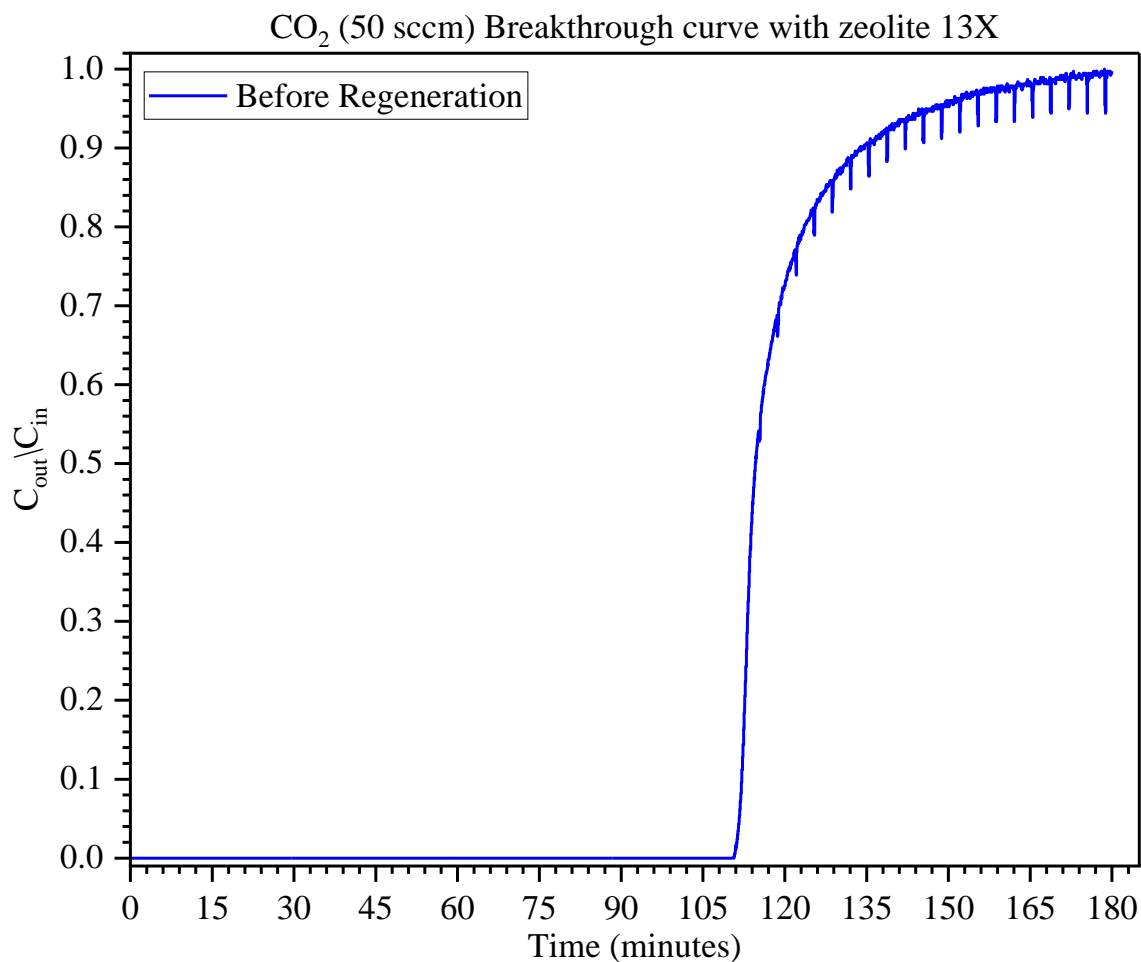
Figure 8. Zeolite 13X CO_2 breakthrough curve at STP conditions before regeneration.

A 90cc stainless steel column containing 60.66 grams of Zeolite 13X was used in the experiment, which was carried out at a temperature of 25°C. It was discovered that the observed adsorption capacity was 4.1 mmol CO_2 per gm of adsorbent as shown in figure 8. The column was subjected to a purging procedure utilizing 100 sccm of nitrogen gas for 4.6 hours after a 15-minute blowdown period at -11.32 PSIG. This went on until the trapped CO2 concentration at the outlet fell to a level that was stable at less than 0.2 sccm.
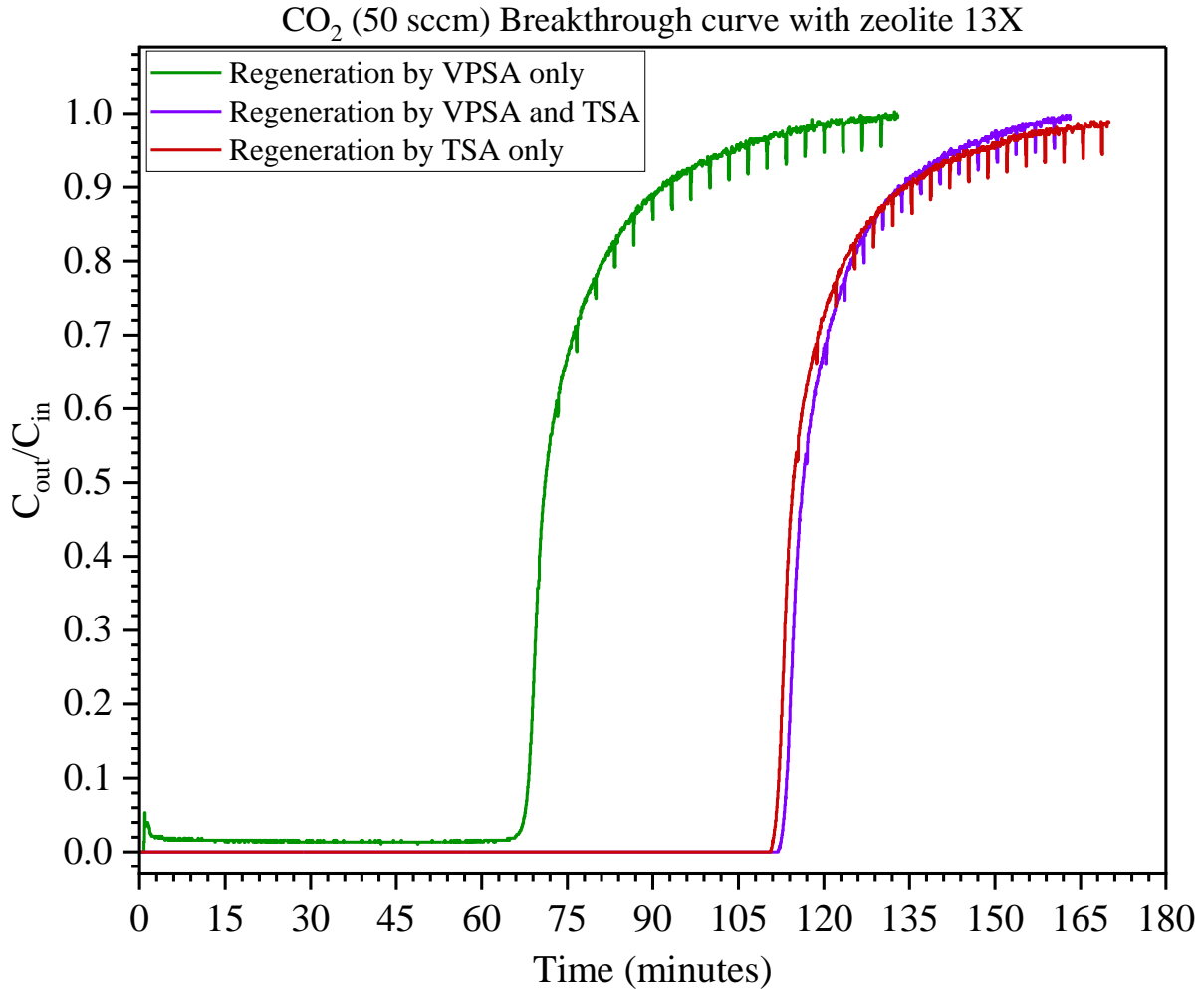
Figure 9. Zeolite 13X CO_2 breakthrough curve at STP conditions after regeneration

After the previously mentioned purging procedure, the column was filled under the same previously mentioned conditions with 50 sccm of N_2 and 50 sccm of CO_2. The adsorption capacity of the adsorbent is determined to be 3.2 mmol CO2 per gm of adsorbent by above mentioned regeneration method of VPSA shown in Figure 8. Furthermore, regeneration by VPSA only, the breakthrough experiment clearly shows the presence of residual CO_2, indicated by small peaks. Therefore, under typical temperature and pressure conditions and single cycle frequency, prolonged purging with nitrogen gas is ineffective in removing CO2 from zeolite 13X.

Upon analyzing the two subsequent cycles of the breakthrough experiment, as illustrated in

Figures 8 and 9, it is noted that Zeolite 13X's adsorption capacity decreases by 21.4% when

regenerating with VPSA only. An additional step is required to regenerate the adsorbent and save

energy during the prolonged purging process due to the observed decrease in adsorption capacity

and the requirement for extended nitrogen purging.

Figure 9 illustrates how TSA alone or in combination with VPSA can restore the adsorption

capacity of zeolite 13X. Before beginning a new breakthrough curve cycle, 120 degrees Celsius

of heat are supplied for 90 minutes during the TSA regeneration process.

7.1.3 Breakthrough curve model fitting
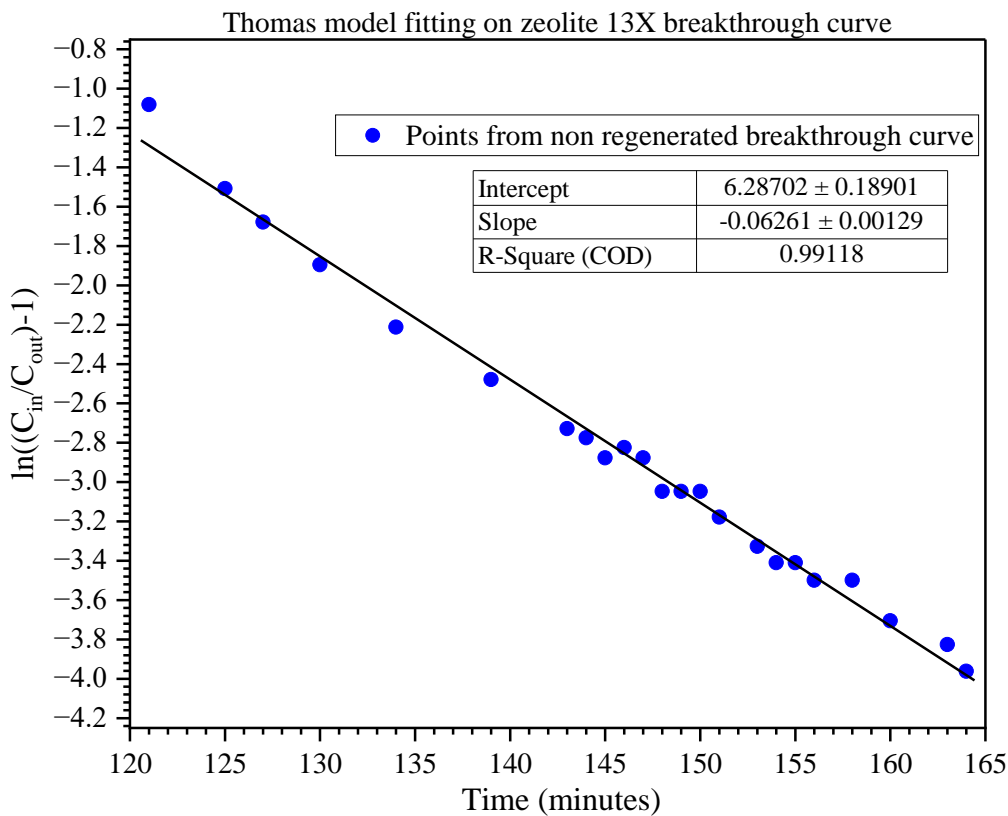
Figure 10: Thomas model fitting on zeolite 13x breakthrough curve at STP conditions

Figure 11: Adam Bohart model fitting on zeolite 13x breakthrough curve at STP conditions
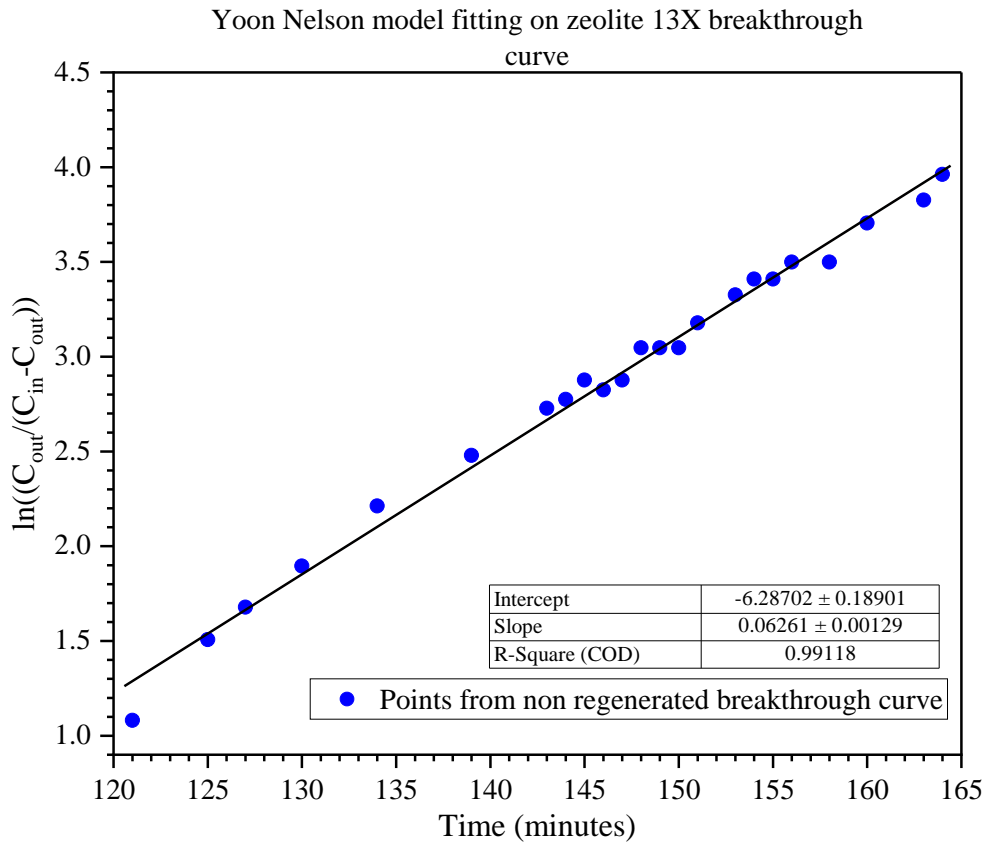
Figure 12: Yoon Nelson model fitting on zeolite 13x breakthrough curve at STP conditions.

According to graphs presented in figures 10, 11, and 12, three different models were employed to fit the breakthrough curve. Among these models, the Yoon-Nelson model and the Thomas model were found to be the most suitable for the given range, exhibiting a high coefficient of determination (R2) value of 0.99. The Adam Bohort model exhibits a lower degree of fit in comparison to the aforementioned models. This finding aligns with the research conducted by Mahanta et al.[111] on the interaction between CO2 and N2 with Zeolite 13X. The observed variability in outcomes can be ascribed to the utilization of distinct types of zeolite and variations in operational parameters.

61

7.2 Activated Carbon

7.2.1 Adsorption capacity by TGA

The adsorption capacity for activated carbon for CO_2 adsorption by TGA is found to be 1.41 mmol of CO_2 / gm adsorbent. Figure 13 depicts the breakthrough curve obtained by TGA experiment.

Figure 13: Breakthrough curve of activated carbon by TGA.

7.2.2 Breakthrough curves by VPSA, TSA and combination

Figure 14: Activated carbon CO_2 breakthrough curve at STP conditions before regeneration.

A 60cc stainless steel column containing 30.78 grams of Zeolite 13X was used in the experiment, which was carried out at a temperature of 25°C. It was discovered that the observed adsorption capacity was 1.17 mmol of CO2/g of adsorbent as shown in figure 14.

Figure 15: Activated carbon CO_2 breakthrough curve at STP conditions after & before regeneration

As was the case with the zeolite 13x that was discussed earlier, the three processes of VPSA,

TSA, and combination experimentation were also carried out on activated carbon. This is

demonstrated in Figure 15, which shows that activated carbon has the ability to regenerate fully

in a single cycle, regardless of the process that is applied. Though, after applying temperature

during regeneration, the adsorption capacity increased slightly to 1.25 mmol of CO2/g of

adsorbent. The observed 7% increase in adsorption capacity may be ascribed to the evaporation

of any trapped water that occurs when temperatures are elevated to 120 degrees Celsius.

7.2.3 Breakthrough curve model fitting
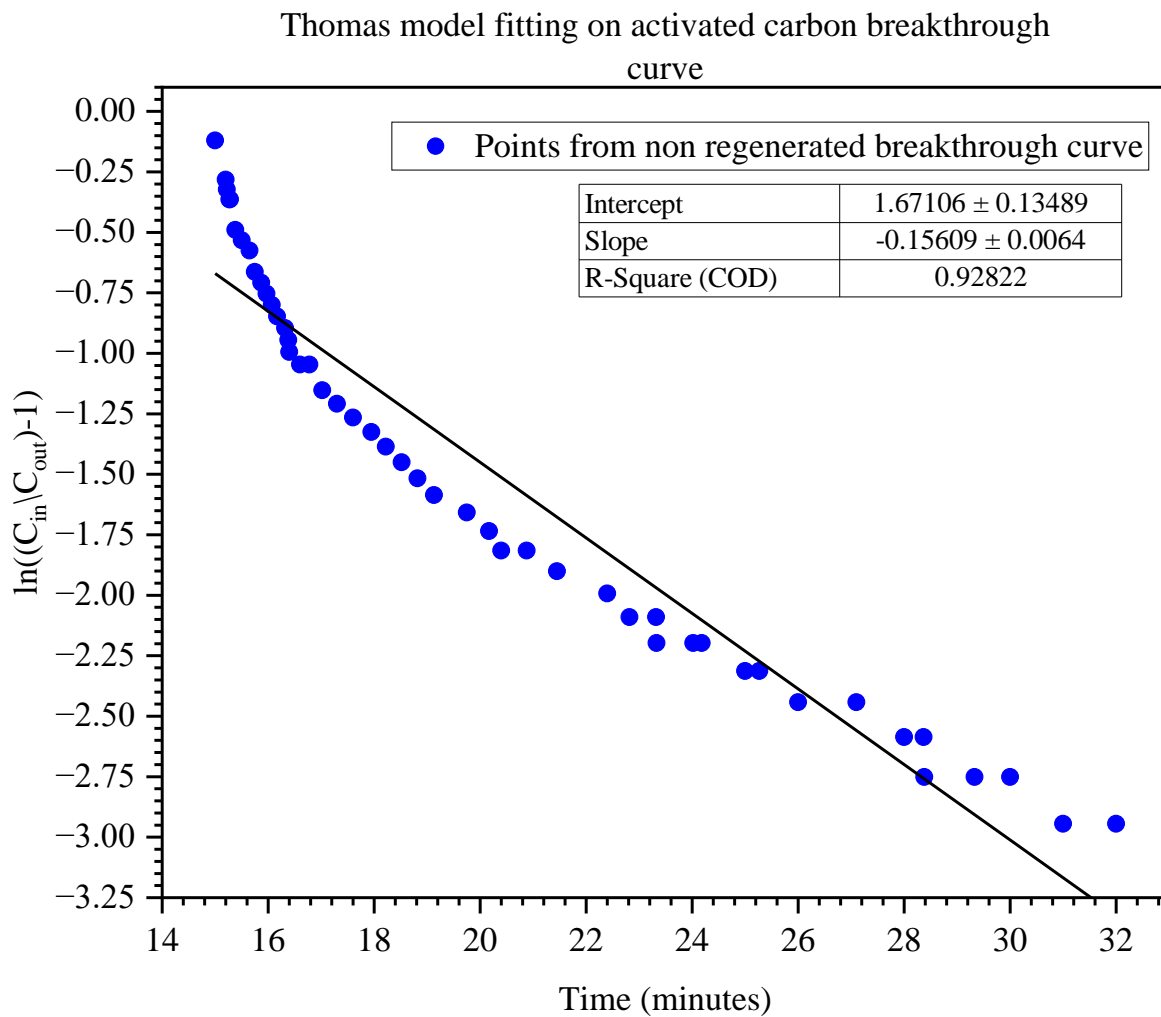
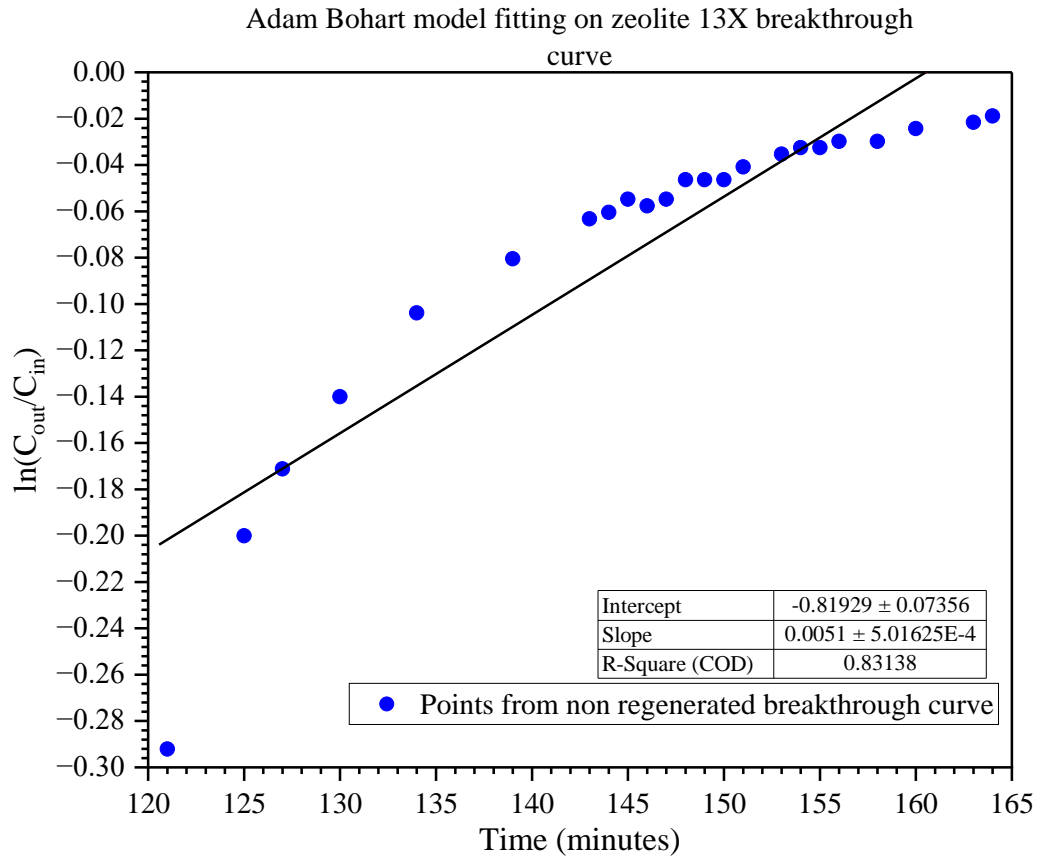Figure 16: Thomas model fitting on activated carbon breakthrough curve at STP conditions
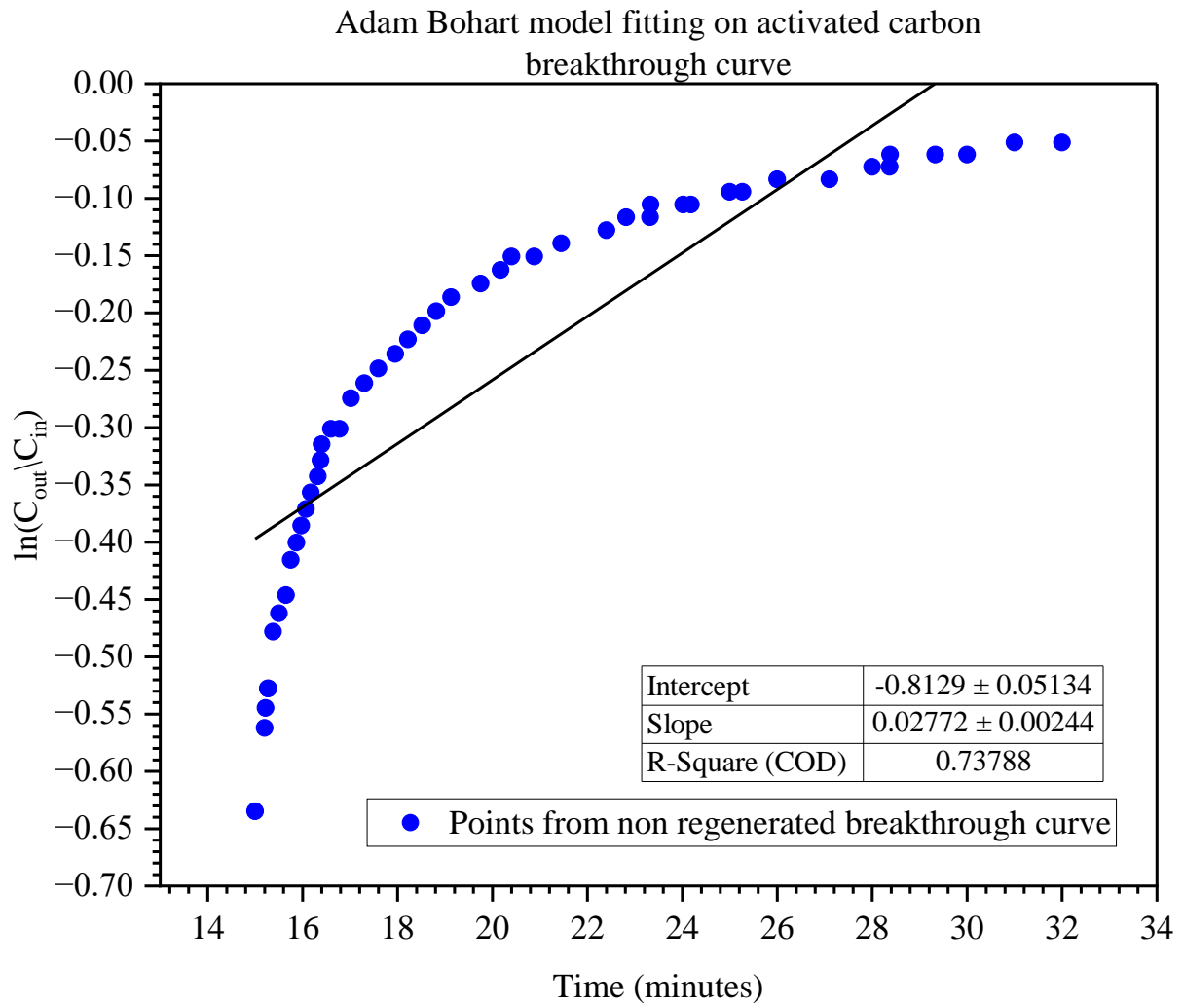
Figure 17: Adam Bohart model fitting on activated carbon breakthrough curve at STP conditions.
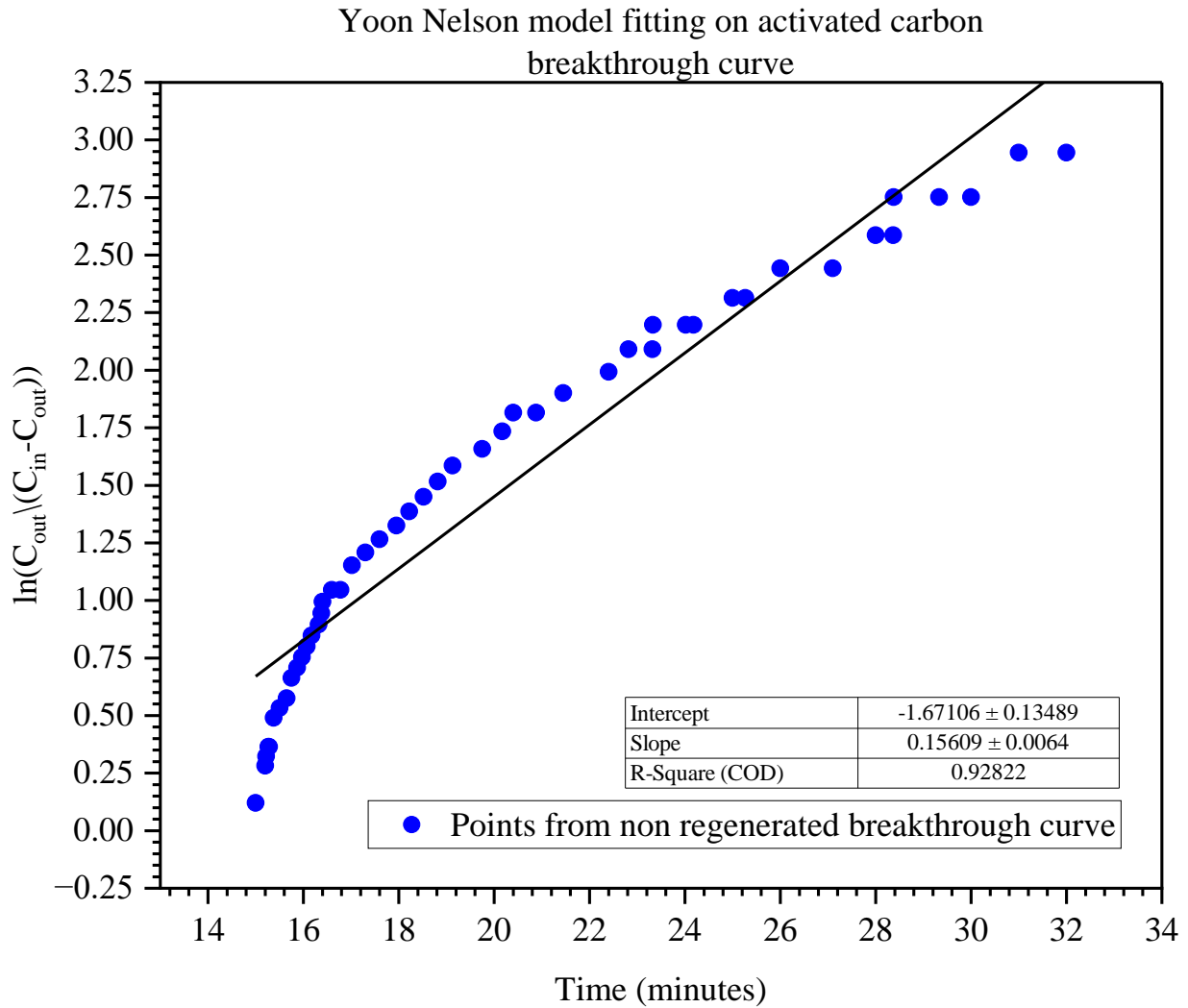
Figure 18: Yoon Nelson model fitting on activated carbon breakthrough curve at STP conditions.

According to the graphs that are shown in figures 16, 17, and 18, three distinct models were utilized in order to fit the breakthrough curve. It was discovered that the Yoon-Nelson model and the Thomas model were the most appropriate for the specified range. Both of these models displayed a high coefficient of determination (R^2) value of 0.92, which indicates that they are the most suitable. When compared to the models that were discussed earlier, the Adam Bohort model demonstrates a lower degree of fit that is 0.73.

7.3 Magnesium Oxide MgO

7.3.1 Adsorption capacity by TGA

The adsorption capacity for magnesium for CO_2 adsorption by TGA is found to be 0.49699 mmol of CO2 / gm adsorbent. Figure 19 depicts the breakthrough curve obtained by TGA experiment.
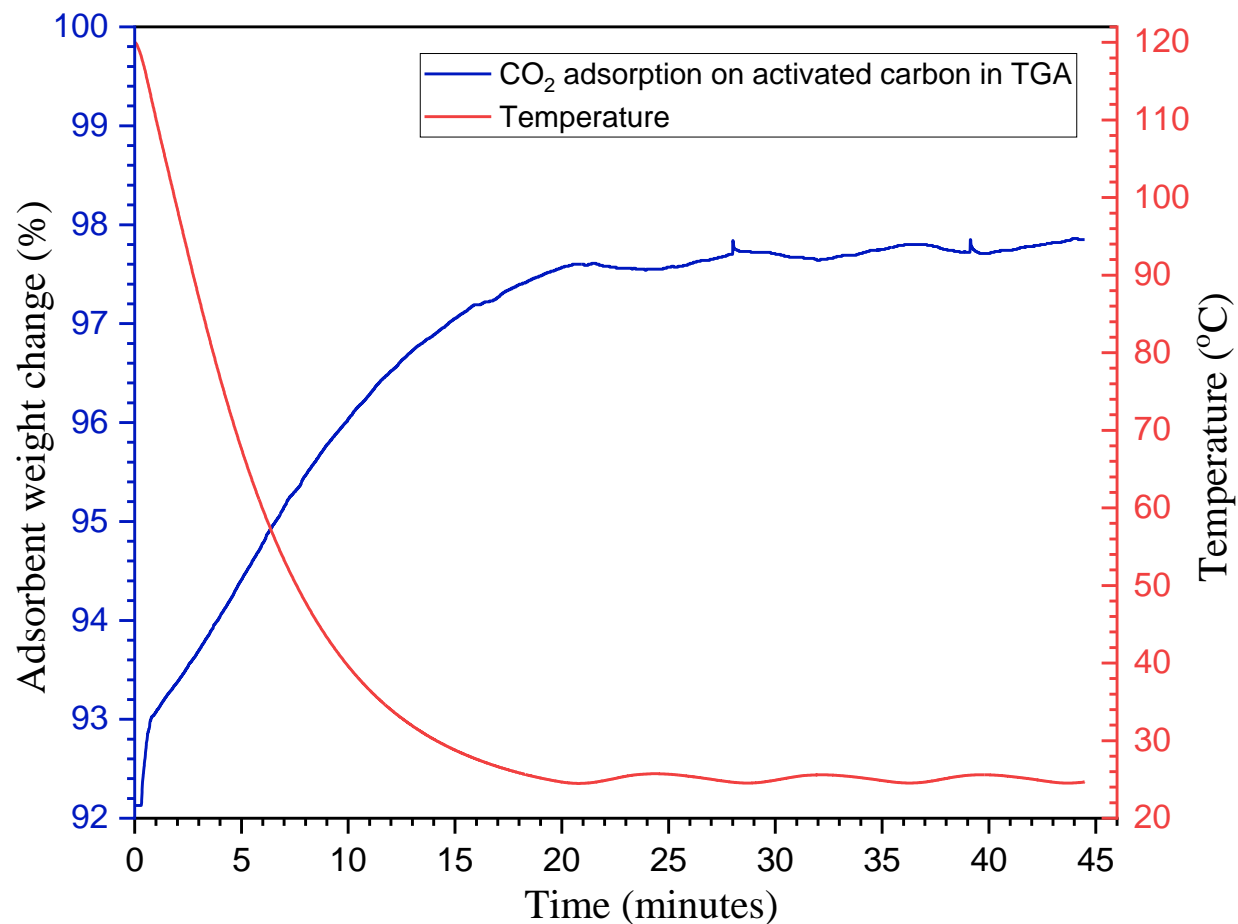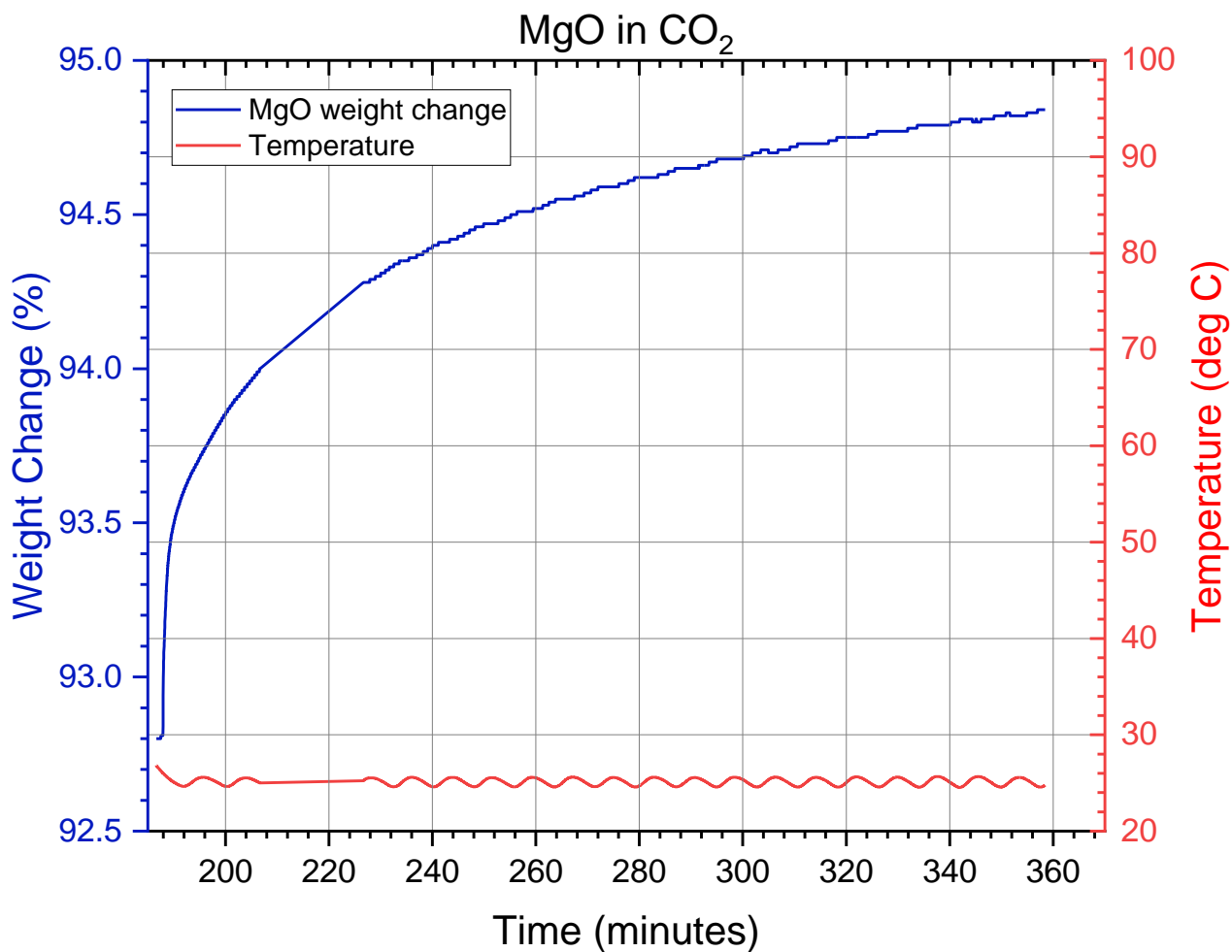

Figure 19: Breakthrough curve of magnesium oxide by TGA
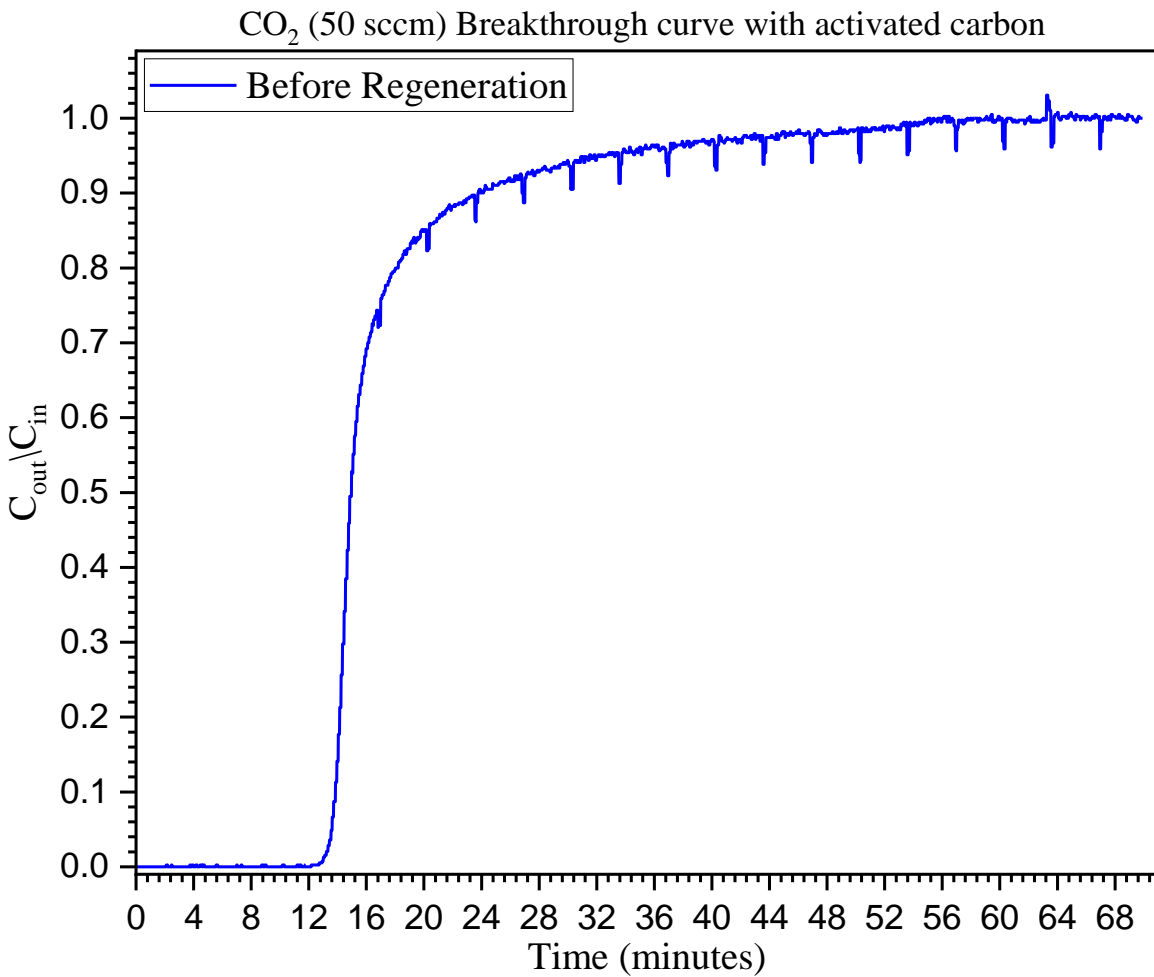
7.3.2 Breakthrough curves by VPSA, TSA and combination
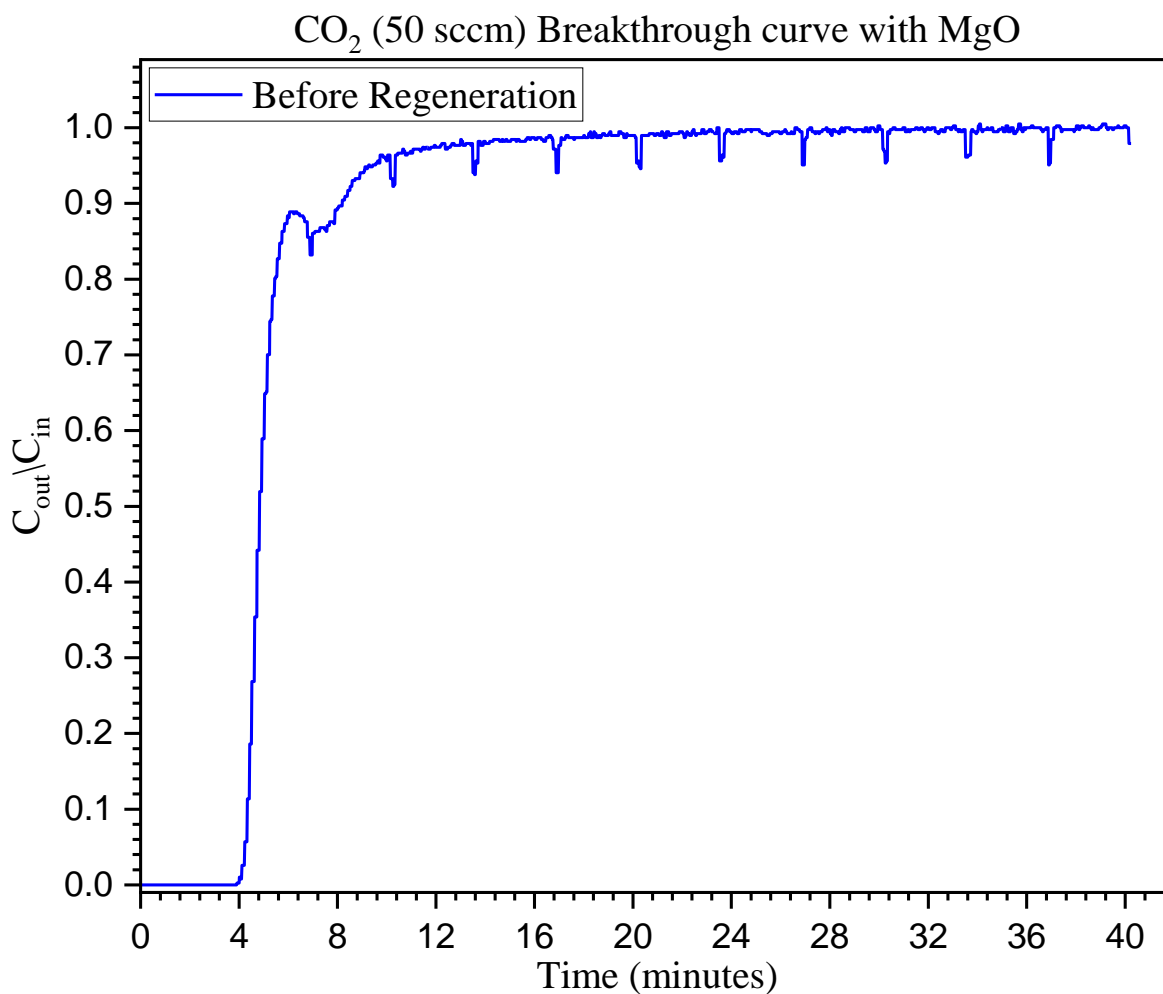
Figure 20: CO$_2$ breakthrough curve with MgO before regeneration at STP conditions.

During the experiment, which was carried out at a temperature of 25 degrees Celsius, a stainless-steel column with a capacity of 90 cubic centimeters and a magnesium oxide content of 26.38 grams was utilized. It was discovered that the observed adsorption capacity was 0.56 mmol of CO2/g of adsorbent as shown in figure 12.
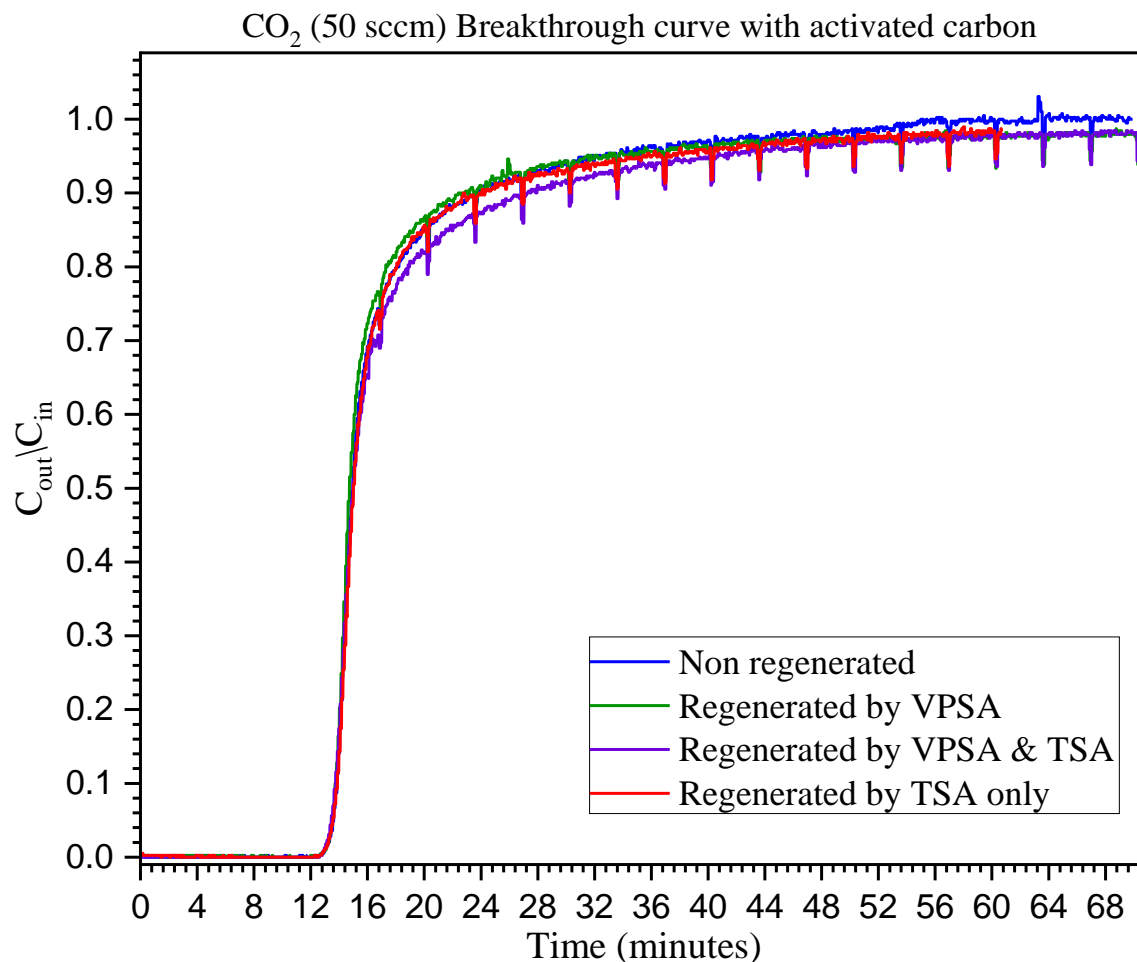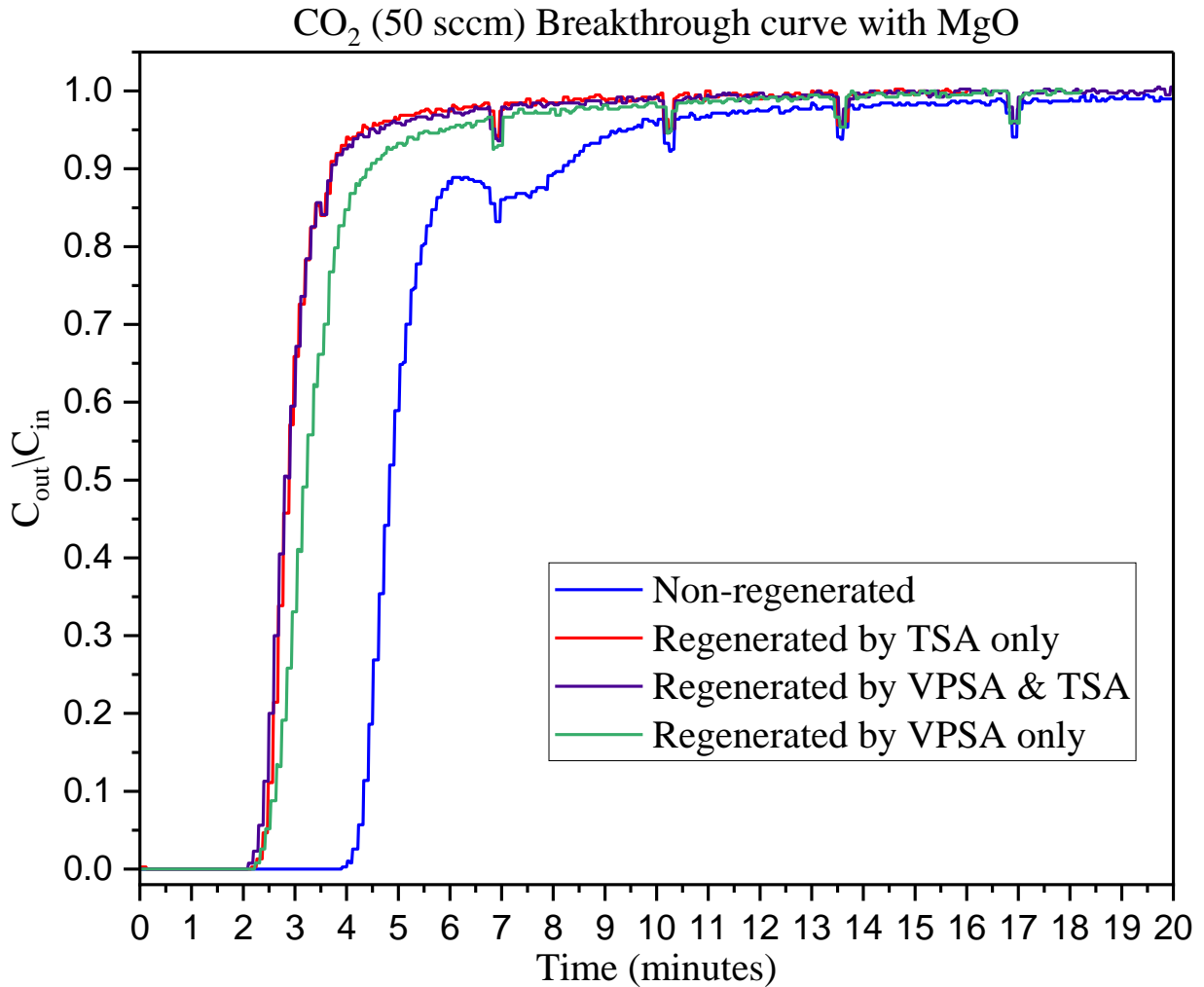
Figure 21: CO$_2$ breakthrough curve with MgO before and after regeneration at STP conditions

In contrast, the adsorbent can regenerate regardless of the regeneration step that is followed when using activated carbon. However, the adsorbent in this instance of magnesium oxide cannot be fully regenerated after applying one cycle of VPSA, TSA, or a combination as seen from figure 21. Following this, the adsorption capacity decreases by 44.5%, or to 0.31 mmol of adsorbed CO2 per gram of MgO.

7.3.3 Breakthrough curve model fitting
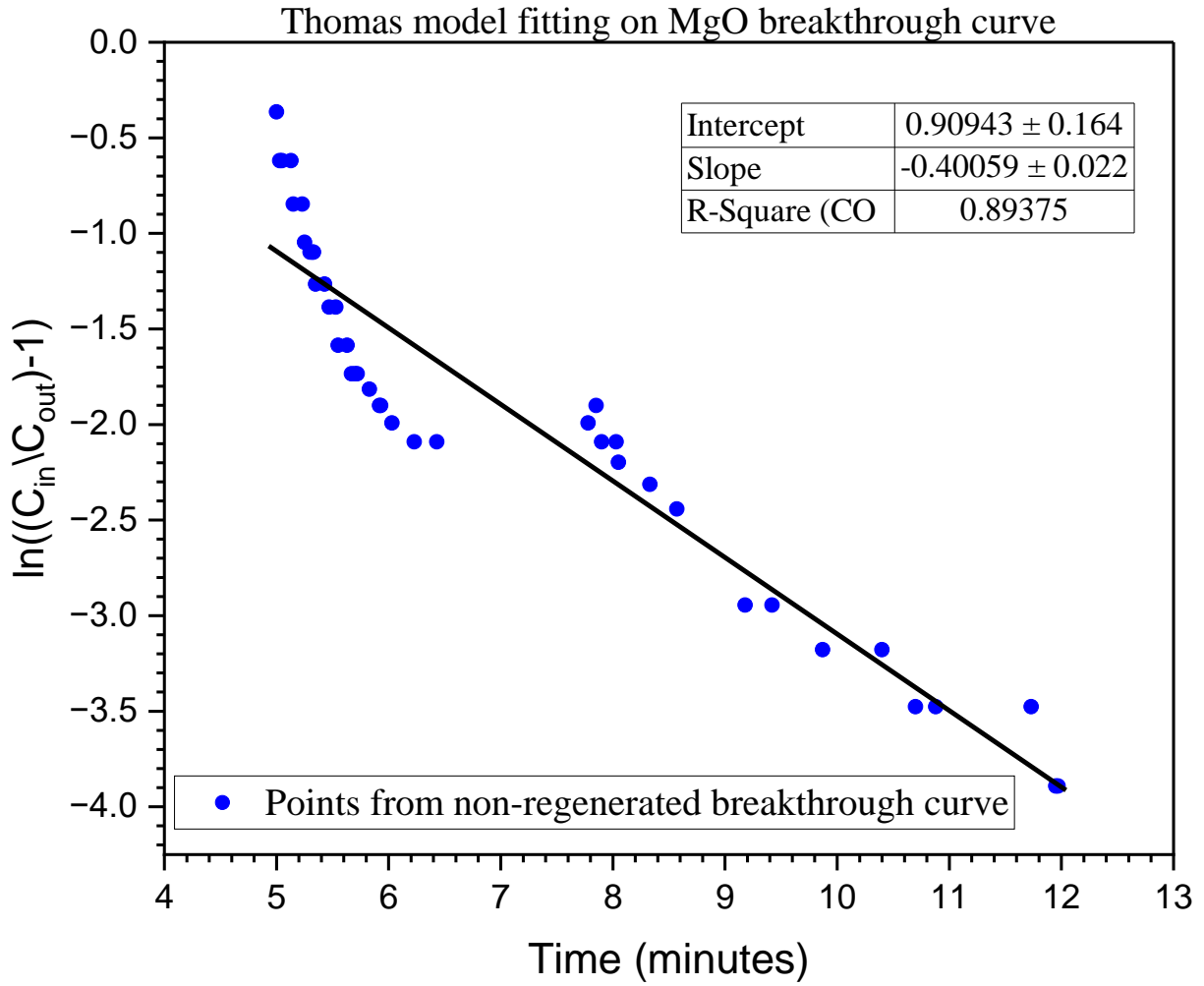
Figure 22: Thomas model fitting on magnesium oxide breakthrough curve at STP conditions.
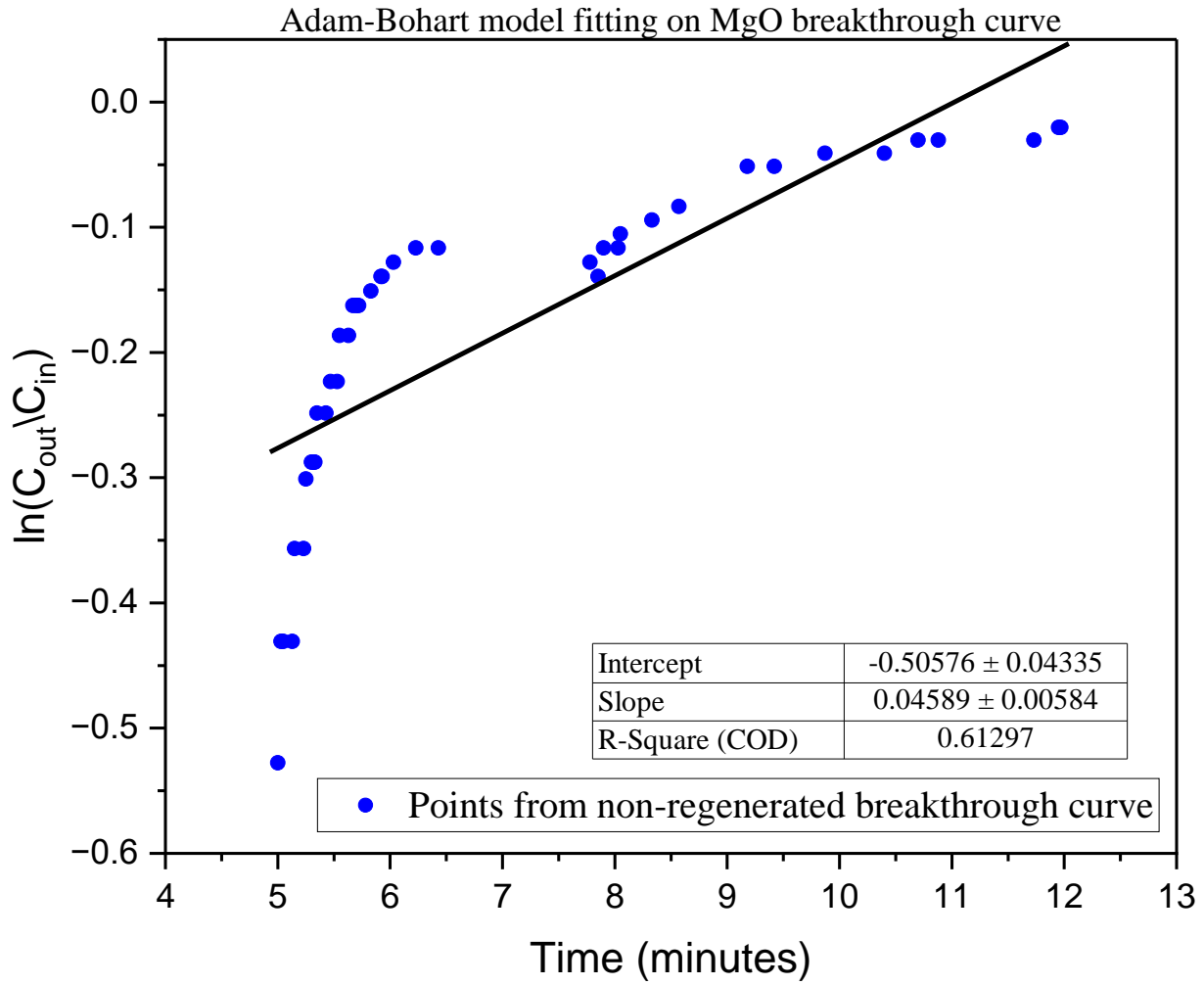
Figure 23: Adam Bohart model fitting on magnesium oxide breakthrough curve at STP condition.
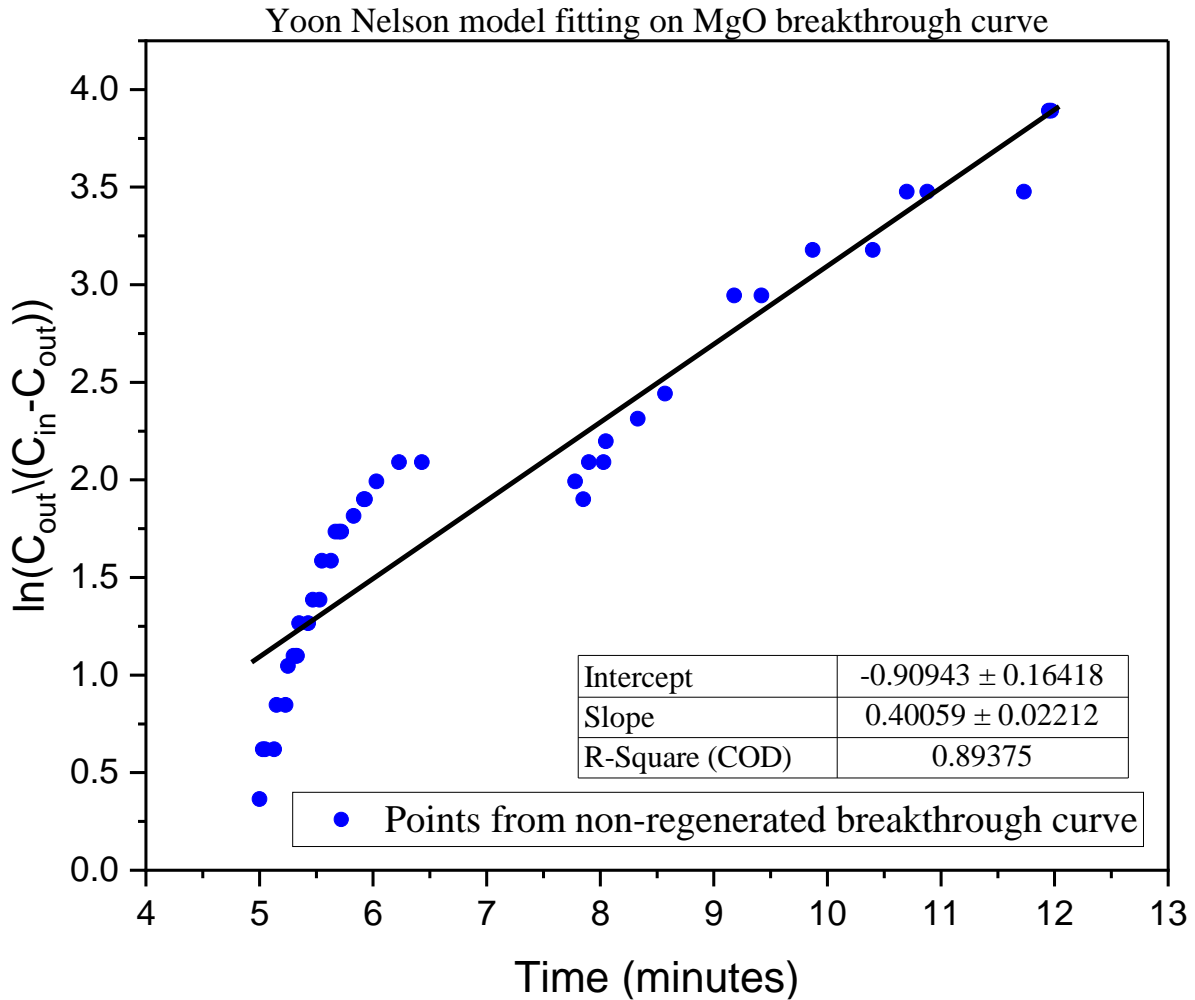
Figure 24: Yoon nelson model fitting on magnesium oxide breakthrough curve at STP conditions.

As can be seen from the graphs in figures 16, 17, and 18, the breakthrough curve was fitted using three different models. It was found that the Thomas and Yoon-Nelson models were the most suitable for the given range. With a high coefficient of determination ($R2$) value of 0.89, both of these models showed that they are the most appropriate. The Adam Bohort model shows a lower degree of fit, 0.61, in comparison to the models that were previously discussed.

Chapter 8

Summary and future work

8.1 Conclusions

1. The most widely available adsorbents—zeolite, activated carbon, and magnesium oxide—were chosen for experimentation through research study. They were selected due to the extensive range of adsorption capacities that their research paper had documented.

2. Commercial zeolite 13X was chosen from among zeolite varieties; it has a pore size radius of 9–10 angstroms and is said to have a higher adsorption capacity in microporous adsorbents than zeolite 3A, zeolite 5A, NaUSY, and other commercially available zeolites.

3. The chosen microporous adsorbents displayed a Type 1 IUPAC isotherm. A combination of Type 1 and Type 5 adsorption isotherms was observed in activated carbon.

4. The BET isotherm, an extended version of the Langmuir isotherm, fits well with selected microporous adsorbents but requires additional steps to calculate specific surface area and pore size volume from the lower relative pressure range of 0.005 to 0.05.

5.As shown in the table 4 below, the first consistency theory was successfully applied to BET isotherms in order to determine specific surface area. The range of specific surface area reported by researchers corresponds to the specific surface area calculated.

Table 4: Textural characteristics of adsorbents

Adsorbent	Specific surface area (m^2/g)	Pore size volume (cc/g)	Specific surface area from research
Zeolite 13x	492 m^2/g	0.270 cc/g	472 m^2/g to 591 m^2/g.[66–74]
Activated carbon	89.44 m²/g	0.3509 cc/g	24 m^2/g to 200 m^2/g[112,113]

Magnesium oxide	59.66 m²/g	0.1113 cc/g	3.4 m^2/g to 203.8 m^2/g[114]

6. The specific surface area of zeolite is the greatest of the three, while magnesium oxide has the smallest surface area to adsorb gas molecules. Activated carbon has a higher pore volume than zeolite 13X but a smaller surface area; this could be due to the presence of mesopores in activated carbon.

7. Two methods were used to obtain breakthrough curves. Where milligrams of adsorbent are required, one can use a thermogravimetric analysis instrument. Another setup was a 90-cc fixed bed adsorption column to obtain a real-time breakthrough curve for CO_2 adsorption.

8. Figure 25 compares breakthrough time for CO_2 adsorption by adsorbents under same STP conditions and before regeneration. As evident from figure 25, zeolite 13X has longer breakthrough time than other two adsorbents.
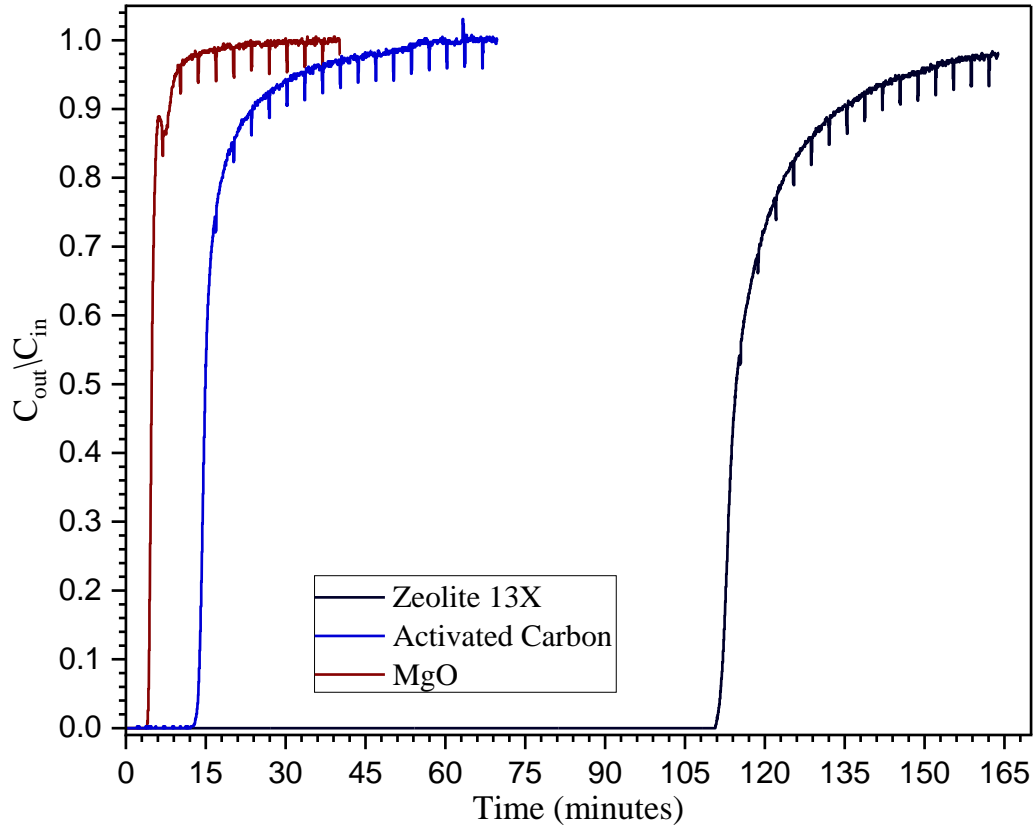
Figure 25: Comparative breakthrough curve for zeolite 13x, activated carbon and magnesium oxide.

9. Table 5 reports the adsorption capacity for co2 adsorption in a 1:1 mixture of co2 and n2 using both fixed bed adsorption and TGA. As can be seen, of the three, zeolite has the largest adsorption capacity. Additionally, it can be seen that the adsorbents' surface areas and adsorption capacities are arranged in the same order, with zeolite having the highest and magnesium oxide having the lowest. it in line with studies that have been reported by other researchers.

Table 5: Adsorption capacity of adsorbent for CO_2 adsorption.

Adsorbent	Adsorption capacity by TGA	Adsorption capacity by fixed bed column	Adsorption capacity by literature review

Zeolite 13x	2.44 mmol of CO_2 per gm	4.1 mmol CO_2 per gm	1.6 mmol/g to 4.6 mmol of CO_2 per gm[115–118]
Activated carbon	1.41 mmol of CO2 / gm adsorbent	1.169413 mmol of CO2/g	1.27 mmol/g to 2.61 mmol of CO_2 per gm[119–122]
Magnesium oxide	0.49699 mmol of CO_2 / gm adsorbent	0.562781 mmol of CO_2/g	0.9 mmol/g to 1 mmol of CO_2 per gm.[123,124]

10. The marginal discrepancy in the adsorption capacity of zeolite 13x between the fixed bed column and TGA can be ascribed to the fluctuating temperature during TGA. A portion of the activated carbon's adsorption capacity by fixed bed columns is caused by moisture that was trapped in the adsorbent and evaporated in the TGA at a high temperature. Due to its unmodified state and the possibility of magnesium carbonate forming on magnesium oxide at high temperatures, the magnesium oxide adsorption capacity is lower than that reported in the literature. The adsorption capacity of MgO from both processes is comparable, as can be observed, because both fixed bed and TGA processes maintain a stable temperature.

11. To regenerate all three adsorbents, VPSA, TSA, or a mix of the two were used. For Zeolite 13x, TSA or a mix of TSA and VPSA is advised for a single cycle of regeneration. On the other hand, all steps remain the same during an activated carbon regeneration cycle, and the material can be fully regenerated. However, it is challenging to fully regenerate MgO using just one cycle of the aforementioned procedure.

12. The breakthrough curves of all three adsorbents were fitted with the Thomas, Adam Bohart, and Yoon Nelson models; the Thomas and Nelson model fits microporous adsorbents better than the Adam Bohart model.

8.2 Future work recommendations

1. In future studies, mesoporous and ultra microporous adsorbents can be investigated and fitted with models of the adsorption equilibrium isotherm.

Incorporating natural adsorbents is also possible.

2. To simulate biogas, it is advised to perform the fixed bed column breakthrough curve experiment using a mixture of methane and nitrogen first, followed by a mixture of methane and carbon dioxide.

3. Major contaminants such as H_2S should be added to gas mixtures going forward, and adsorbents for their removal should be investigated.

Since moisture is frequently present in biogas, detailed experiments to release trapped water can be carried out.

4.Magnesium oxide has a lower specific surface area and adsorption capacity, so it may be possible to increase these by exploring new methods of synthesizing MgO.

5.To determine the regeneration potential and capability of adsorbents, a detailed analysis of the regeneration of adsorbents using VPSA, TSA, and their combination can be conducted at a higher regeneration frequency.

6.sTo improve biogas by eliminating contaminants, strategies for optimizing process parameters such as feed flow, temperature, and vacuum pressure should be developed in order to reduce costs and energy penalty.

References

1.   Weiland, P. Biogas production: current state and perspectives. *Appl Microbiol Biotechnol* **85**, 849–860 (2010).

2.   Nizami, A. S. *et al.* Waste biorefineries: Enabling circular economies in developing countries. *Bioresource Technology* **241**, 1101–1117 (2017).

3.   Sahota, S. *et al.* Review of trends in biogas upgradation technologies and future perspectives. *Bioresource Technology Reports* **1**, 79–88 (2018).

4.   IRENA: Biogas for road vehicles: Technology brief - Google Scholar. https://scholar.google.com/scholar_lookup?title=Biogas%20for%20Road%20Vehicles%20Techn ology%20Brief&publication_year=2017&author=IRENA%20(International%20Renewable%20 Energy%20Agency).

5.   Esteves, I. A. A. C., Lopes, M. S. S., Nunes, P. M. C. & Mota, J. P. B. Adsorption of natural gas and biogas components on activated carbon. *Separation and Purification Technology* **62**, 281–296 (2008).

6.   Burchell, T. & Rogers, M. Low Pressure Storage of Natural Gas for Vehicular Applications. *SAE Transactions* **109**, 2242–2246 (2000).

7.   Bansal, T., Tripathi, N. & Chawla, G. Upgradation of biogas using combined method of alkaline water scrubbing and adsoption through carbon molecular sieve. *International Journal of ChemTech Research* **5**, 886–890 (2013).

8.   Persson, M., Jönsson, O. & Wellinger, A. Biogas upgrading to vehicle fuel standards and grid injection. in *IEA Bioenergy task* vol. 37 1–34 (2006).

9.   Berdugo, T. & Coutiño, A. M. Barriers and solutions to the successful diffusion of dual-fuel trucks in Europe. (2011).

10.   Sahota, S. *et al.* Characterization of leaf waste based biochar for cost effective hydrogen sulphide removal from biogas. *Bioresource Technology* **250**, 635–641 (2018).

11.   Bauer, F., Persson, T., Hulteberg, C. & Tamm, D. Biogas upgrading – technology overview, comparison and perspectives for the future. *Biofuels, Bioproducts and Biorefining* **7**, 499–511 (2013).

12.   Yang, R. T. *Gas Separation By Adsorption Processes*. (World Scientific, 1997).

13.   Bae, Y.-S. *et al.* Separation of CO2 from CH4 Using Mixed-Ligand Metal−Organic Frameworks. *Langmuir* **24**, 8592–8598 (2008).

14.   Finsy, V. *et al.* Separation of CO2/CH4 mixtures with the MIL-53(Al) metal–organic framework. *Microporous and Mesoporous Materials* **120**, 221–227 (2009).

15.   Bastin, L. *et al.* A Microporous Metal−Organic Framework for Separation of CO2/N2 and CO2/CH4 by Fixed-Bed Adsorption. *J. Phys. Chem. C* **112**, 1575–1581 (2008).

16.   Development and Evaluation of Porous Materials for Carbon Dioxide Separation and Capture - Bae - 2011 - Angewandte Chemie International Edition - Wiley Online Library. https://onlinelibrary.wiley.com/doi/abs/10.1002/anie.201101891?casa_token=7atX4ZWufe4AA AAA:1q4QDENb30WSxVjthTp5mHuAzCgqTuHW2BRG5K9YCuhooK6FTTVw6L9JnZRY5if RHmKBn5zi2N78Vw.

17.   Tagliabue, M. *et al.* Natural gas treating by selective adsorption: Material science and chemical engineering interplay. *Chemical Engineering Journal* **155**, 553–566 (2009).

18.   Knaebel, K. S. Adsorbent selection. *Accessed on* **6**, (2011).

19.   Peredo-Mancilla, D. *et al.* Comparative study of the CH4/CO2 adsorption selectivity of activated carbons for biogas upgrading. *Journal of Environmental Chemical Engineering* **7**, 103368 (2019).

20.   Do Duong, D. *Adsorption analysis: equilibria and kinetics*. (Imperial College Press, 1998).

21.   Adsorption separation of CO2/CH4 gas mixture on the commercial zeolites at atmospheric pressure - ScienceDirect. https://www.sciencedirect.com/science/article/pii/S1385894713007407?via%3Dihub.

22.   An overview on trace CO2 removal by advanced physisorbent materials - ScienceDirect. https://www.sciencedirect.com/science/article/pii/S0301479719315920?via%3Dihub.

23.   Pressure swing adsorption for biogas upgrading. A new process configuration for the separation of biomethane and carbon dioxide - ScienceDirect. https://www.sciencedirect.com/science/article/pii/S0959652616316110?via%3Dihub.

24.   Arya, A. *et al.* Upgrading Biogas at Low Pressure by Vacuum Swing Adsorption. *Ind. Eng. Chem. Res.* **54**, 404–413 (2015).

25.   Burchell, T. D. *Carbon materials for advanced technologies*. (Elsevier, 1999).

26.   Ruhaimi, A. H., Aziz, M. A. A. & Jalil, A. A. Magnesium oxide-based adsorbents for carbon dioxide capture: Current progress and future opportunities. *Journal of CO2 Utilization* **43**, 101357 (2021).

27.   Creamer, A. E., Gao, B., Zimmerman, A. & Harris, W. Biomass-facilitated production of activated magnesium oxide nanoparticles with extraordinary CO2 capture capacity. *Chemical Engineering Journal* **334**, 81–88 (2018).

28.   Bhagiyalakshmi, M., Lee, J. Y. & Jang, H. T. Synthesis of mesoporous magnesium oxide: Its application to CO2 chemisorption. *International Journal of Greenhouse Gas Control* **4**, 51–56 (2010).

29.   Ruthven, D. M. *Principles of Adsorption and Adsorption Processes*. (John Wiley & Sons, 1984).

30.   Bonjour, J., Chalfen, J.-B. & Meunier, F. Temperature Swing Adsorption Process with Indirect Cooling and Heating. *Ind. Eng. Chem. Res.* **41**, 5802–5811 (2002).

31.   Kong, L. & Adidharma, H. A new adsorption model based on generalized van der Waals partition function for the description of all types of adsorption isotherms. *Chemical Engineering Journal* **375**, 122112 (2019).

32.   Al-Ghouti, M. A. & Da'ana, D. A. Guidelines for the use and interpretation of adsorption isotherm models: A review. *Journal of Hazardous Materials* **393**, 122383 (2020).

33.   Ghani, W. A. W. A. K. Langmuir model application on solid-liquid adsorption using agricultural wastes: Environmental application review.

34.   Ayawei, N., Ebelegi, A. N. & Wankasi, D. Modelling and Interpretation of Adsorption Isotherms. *Journal of Chemistry* **2017**, e3039817 (2017).

35.   Yan, X.-F., Fan, X.-R., Wang, Q. & Shen, Y. An adsorption isotherm model for adsorption performance of silver-loaded activated carbon. *Thermal Science* **21**, 48–48 (2017).

36.   Keller, J. & Staudt, R. Gas Adsorption Equilibria: Experimental Methods and Adsorption Isotherms. *Geomagnetizm i Aeronomiia* (2004).

37.   Sing, K. S. W. Reporting physisorption data for gas/solid systems with special reference to the determination of surface area and porosity (Recommendations 1984). *Pure Appl. Chem.* **57**, 603–619 (1985).

38.   Thommes, M. *et al.* Physisorption of gases, with special reference to the evaluation of surface area and pore size distribution (IUPAC Technical Report). *Pure and Applied Chemistry* **87**, 1051–1069 (2015).

39.   Khalfaoui, M., Knani, S., Hachicha, M. A. & Ben Lamine, A. New theoretical expressions for the five adsorption type isotherms clasified by BET based on statistical physics treatment. *Journal of colloid and interface science* **263**, 350–6 (2003).

40.   Inglezakis, V. J., Poulopoulos, S. G. & Kazemian, H. Insights into the S-shaped sorption isotherms and their dimensionless forms. *Microporous and Mesoporous Materials* **272**, 166–176 (2018).

41.   Muhammad Sultan. Optimization of adsorption isotherm types for desiccant air-conditioning applications | Request PDF. https://www.researchgate.net/publication/322575267_Optimization_of_adsorption_isotherm_typ es_for_desiccant_air-conditioning_applications.

42.   Thommes, M. *et al.* Physisorption of gases, with special reference to the evaluation of surface area and pore size distribution (IUPAC Technical Report). *Pure and Applied Chemistry* **87**, 1051–1069 (2015).

43.   Wang, G. *et al.* Gaseous adsorption of hexamethyldisiloxane on carbons: Isotherms, isosteric heats and kinetics. *Chemosphere* **247**, 125862 (2020).

44.   Donohue, M. D. & Aranovich, G. L. Adsorption Hysteresis in Porous Solids. *Journal of Colloid and Interface Science* **205**, 121–130 (1998).

45.   Kadlec, O. & Dubinin, M. M. Comments on the limits of applicability of the mechanism of capillary condensation. *Journal of Colloid and Interface Science* **31**, 479–489 (1969).

46.   Mason, G. & Everett, D. H. A model of adsorption-desorption hysteresis in which hysteresis is primarily developed by the interconnections in a network of pores. *Proceedings of the Royal Society of London. A. Mathematical and Physical Sciences* **390**, 47–72 (1997).

47.   Mahmoud, D. K., Salleh, M. A. M., Karim, W. A. W. A., Idris, A. & Abidin, Z. Z. Batch adsorption of basic dye using acid treated kenaf fibre char: Equilibrium, kinetic and thermodynamic studies. *Chemical Engineering Journal* **181–182**, 449 (2012).

48.   Physisorption theory of surface area and porosity determination: A short review | AIP Conference Proceedings | AIP Publishing. https://pubs.aip.org/aip/acp/article-abstract/2450/1/020007/2824046/Physisorption-theory-of-surface-area-and-porosity?redirectedFrom=fulltext.

49.   Sing, K. The use of nitrogen adsorption for the characterisation of porous materials. *Colloids and Surfaces A: Physicochemical and Engineering Aspects* **187–188**, 3–9 (2001).

50.   Alafnan, S. *et al.* Langmuir adsorption isotherm in unconventional resources: Applicability and limitations. *Journal of Petroleum Science and Engineering* **207**, 109172 (2021).

51.   Fan, Z., Hou, J., Ge, X., Zhao, P. & Liu, J. Investigating Influential Factors of the Gas Absorption Capacity in Shale Reservoirs Using Integrated Petrophysical, Mineralogical and Geochemical Experiments: A Case Study. *Energies* **11**, 3078 (2018).

52.   David C. Koopman. Assumption of local equilibrium in adsorption processes - Koopman - 1992 - AIChE Journal - Wiley Online Library. https://aiche.onlinelibrary.wiley.com/doi/abs/10.1002/aic.690380418?casa_token=z8B64VFmb9 AAAAAA:j__JagrOv4OReDS2P_DOSS9L6KXKVSSRXH1A_A8T4UXe2fFnGlHWEf1eFeY5 kGL_VnL4mi3FUk17wA.

53.   Zhang, T., Ellis, G. S., Ruppel, S. C., Milliken, K. & Yang, R. Effect of organic-matter type and thermal maturity on methane adsorption in shale-gas systems. *Organic Geochemistry* **47**, 120–131 (2012).

54.   Ye, W. *et al.* Chapter 3 - Design with modeling techniques. in *Industrial Ventilation Design Guidebook (Second Edition)* (eds. Goodfellow, H. D. & Wang, Y.) 109–183 (Academic Press, 2021). doi:10.1016/B978-0-12-816673-4.00008-0.

55.   Saadi, R., Saadi, Z., Fazaeli, R. & Fard, N. E. Monolayer and multilayer adsorption isotherm models for sorption from aqueous media. *Korean J. Chem. Eng.* **32**, 787–799 (2015).

56.   D6556 Standard Test Method for Carbon Black—Total and External Surface Area by Nitrogen Adsorption. https://www.astm.org/d6556-21.html.

57.   Physical Chemistry of Surfaces, 6th Edition | Wiley. *Wiley.com* https://www.wiley.com/en-gb/Physical+Chemistry+of+Surfaces%2C+6th+Edition-p-9780471148739.

58.   Chen, X. Modeling of Experimental Adsorption Isotherm Data. *Information* **6**, 14–22 (2015).

59.   Ho, Y. S., Porter, J. F. & McKay, G. Equilibrium Isotherm Studies for the Sorption of Divalent Metal Ions onto Peat: Copper, Nickel and Lead Single Component Systems. *Water, Air, & Soil Pollution* **141**, 1–33 (2002).

60.   Frontiers | Tailoring Low-Cost Granular Activated Carbons Intended for CO2 Adsorption. https://www.frontiersin.org/articles/10.3389/fchem.2020.581133/full.

61.   CO2 adsorption on zeolite X/activated carbon composites | Adsorption. https://link.springer.com/article/10.1007/s10450-012-9440-0.

62.   Kasikamphaiboon, P. & Khunjan, U. CO_2 Adsorption from Biogas Using Amine-Functionalized MgO. *International Journal of Chemical Engineering* **2018**, e1706405 (2018).

63.   Qazvini, O. T., Babarao, R. & Telfer, S. G. Selective capture of carbon dioxide from hydrocarbons using a metal-organic framework. *Nat Commun* **12**, 197 (2021).

64.   Bae, Y.-S. & Snurr, R. Q. Development and Evaluation of Porous Materials for Carbon Dioxide Separation and Capture. *Angewandte Chemie International Edition* **50**, 11586–11596 (2011).

65.   Gholipour, F. & Mofarahi, M. Adsorption equilibrium of methane and carbon dioxide on zeolite 13X: Experimental and thermodynamic modeling. *The Journal of Supercritical Fluids* **111**, 47–54 (2016).

66.   Wang, J.-Q., Huang, Y.-X., Pan, Y. & Mi, J.-X. Hydrothermal synthesis of high purity zeolite A from natural kaolin without calcination. *Microporous and Mesoporous Materials* **199**, 50–56 (2014).

67.   Ma, Y. *et al.* Synthesis and characterization of 13X zeolite from low-grade natural kaolin. *Advanced Powder Technology* **25**, 495–499 (2014).

68.   Chen, D. *et al.* Synthesis and characterization of zeolite X from lithium slag. *Applied Clay Science* **59–60**, 148–151 (2012).

69.   Kazemian, H., Naghdali, Z., Ghaffari Kashani, T. & Farhadi, F. Conversion of high silicon fly ash to Na-P1 zeolite: Alkaline fusion followed by hydrothermal crystallization. *Advanced Powder Technology* **21**, 279–283 (2010).

70.   Purnomo, C. W., Salim, C. & Hinode, H. Synthesis of pure Na–X and Na–A zeolite from bagasse fly ash. *Microporous and Mesoporous Materials* **162**, 6–13 (2012).

71.   Wajima, T. *et al.* Zeolite synthesis from paper sludge ash at low temperature (90°C) with addition of diatomite. *Journal of Hazardous Materials* **132**, 244–252 (2006).

72.   Fernandes Machado, N. R. C. & Malachini Miotto, D. M. Synthesis of Na–A and –X zeolites from oil shale ash. *Fuel* **84**, 2289–2294 (2005).

73.   Tanaka, H. & Fujii, A. Effect of stirring on the dissolution of coal fly ash and synthesis of pure-form Na-A and -X zeolites by two-step process. *Advanced Powder Technology* **20**, 473–479 (2009).

74.   Garshasbi, V., Jahangiri, M. & Anbia, M. Equilibrium CO2 adsorption on zeolite 13X prepared from natural clays. *Applied Surface Science* **393**, 225–233 (2017).

75.   Barrett, E. P., Joyner, L. G. & Halenda, P. P. The Determination of Pore Volume and Area Distributions in Porous Substances. I. Computations from Nitrogen Isotherms. *J. Am. Chem. Soc.* **73**, 373–380 (1951).

76.   Musa, M. A., Yin, C.-Y. & Savory, R. M. Analysis of the textural characteristics and pore size distribution of a commercial zeolite using various adsorption models. *Journal of Applied Sciences* **11**, 3650–3654 (2011).

77.   Horváth, G. & Kawazoe, K. Method for the calculation of effective pore size distribution in molecular sieve carbon. *Journal of Chemical Engineering of Japan* **16**, 470–475 (1983).

78.   Evans, R. & Tarazona, P. Theory of Condensation in Narrow Capillaries. *Phys. Rev. Lett.* **52**, 557–560 (1984).

79.   Bezerra, D. P., Oliveira, R. S., Vieira, R. S., Cavalcante, C. L. & Azevedo, D. C. S. Adsorption of CO2 on nitrogen-enriched activated carbon and zeolite 13X. *Adsorption* **17**, 235–246 (2011).

80.   Seraj, S., Ferron, R. D. & Juenger, M. C. G. Calcining natural zeolites to improve their effect on cementitious mixture workability. *Cement and Concrete Research* **85**, 102–110 (2016).

81.   Mockovčiaková, A., Matik, M., Orolínová, Z., Hudec, P. & Kmecová, E. Structural characteristics of modified natural zeolite. *J Porous Mater* **15**, 559–564 (2008).

82.   Mansouri, N., Rikhtegar, N., Panahi, H. A., Atabi, F. & Shahraki, B. K. Porosity, characterization and structural properties of natural zeolite-clinoptilolite-as a sorbent. *Environment Protection Engineering* **39**, 139–152 (2013).

83.   Rodriguez-Reinoso, Francisco., Martin-Martinez, J. Miguel., Prado-Burguete, Celia. & McEnaney, Brian. A standard adsorption isotherm for the characterization of activated carbons. *J. Phys. Chem.* **91**, 515–516 (1987).

84.   Yazaydın, A. Ö. *et al.* Screening of Metal−Organic Frameworks for Carbon Dioxide Capture from Flue Gas Using a Combined Experimental and Modeling Approach. *J. Am. Chem. Soc.* **131**, 18198–18199 (2009).

85.   Bhatnagar, A., Vilar, V. J. P., Botelho, C. M. S. & Boaventura, R. A. R. Coconut-based biosorbents for water treatment — A review of the recent literature. *Advances in Colloid and Interface Science* **160**, 1–15 (2010).

86.   Thitame, P. V. & Shukla, S. R. Adsorptive removal of reactive dyes from aqueous solution using activated carbon synthesized from waste biomass materials. *Int. J. Environ. Sci. Technol.* **13**, 561–570 (2016).

87.   Amine modification on kaolinites to enhance CO2 adsorption. *Journal of Colloid and Interface Science* **436**, 47–51 (2014).

88.   Patel, H. Fixed-bed column adsorption study: a comprehensive review. *Appl Water Sci* **9**, 45 (2019).

89.   Monash, P. & Pugazhenthi, G. Removal of Crystal Violet Dye from Aqueous Solution Using Calcined and Uncalcined Mixed Clay Adsorbents. *Separation Science and Technology* **45**, 94–104 (2009).

90.   Cavalcante: Industrial adsorption separation processes:... - Google Scholar. https://scholar.google.com/scholar_lookup?&title=Industrial%20adsorption%20separation%20pr ocesses%3A%20fundamentals%2C%20modeling%20and%20applications&journal=Latin%20A m%20Appl%20Res&volume=30&pages=357-364&publication_year=2000&author=Cavalcante%2CCL.

91.   *Control of Organic Substances in Water and Wastewater*. (Office of Research and Development, U.S. Environmental Protection Agency, 1983).

92.   Gupta, V. K. & Ali, I. *Environmental water: advances in treatment, remediation and recycling*. (Newnes, 2012).

93.   Crittenden: Adsorption technology and design - Google Scholar. https://scholar.google.com/scholar_lookup?&title=Adsorption%20technology%20and%20design %2C%20Chapter%205%3A%20Processes%20and%20cycles&pages=96-133&publication_year=1998&author=Crittenden%2CB&author=Thomas%2CWJ.

94.   Moyo, M., Pakade, V. E. & Modise, S. J. Biosorption of lead(II) by chemically modified Mangifera indica seed shells: Adsorbent preparation, characterization and performance assessment. *Process Safety and Environmental Protection* **111**, 40–51 (2017).

95.   Modeling and analysis of a packed-bed column for the effective removal of zinc from aqueous solution using dual surface-modified biomass: Particulate Science and Technology: Vol 36, No 8. https://www.tandfonline.com/doi/abs/10.1080/02726351.2017.1329243.

96.   Study of a fixed-bed column in the adsorption of an azo dye from an aqueous medium using a chitosan–glutaraldehyde biosorbent - Jaime López-Cervantes, Dalia I Sánchez-Machado, Reyna G Sánchez-Duarte, Ma A Correa-Murrieta, 2018. https://journals.sagepub.com/doi/10.1177/0263617416688021.

97.   Ahmad, A. A. & Hameed, B. H. Fixed-bed adsorption of reactive azo dye onto granular activated carbon prepared from waste. *Journal of Hazardous Materials* **175**, 298–303 (2010).

98.   Mesoporous/microporous silica materials: Preparation from natural sands and highly efficient fixed-bed adsorption of methylene blue in wastewater - ScienceDirect. https://www.sciencedirect.com/science/article/pii/S1387181117305590?casa_token=OxGMHZej TTMAAAAA:ZyqOb_Kl8W4g7aI94DPW9T_7hA_g-hPNHpmJn1vqwtnIGZF3AatBTdY5J8B8Dm5PPr1ZttPCTw.

99.   Fat'hi, M. R., Asfaram, A., Hadipour, A. & Roosta, M. Kinetics and thermodynamic studies for removal of acid blue 129 from aqueous solution by almond shell. *J Environ Health Sci Engineer* **12**, 62 (2014).

100.   Leaching of ammonium and nitrate from Acrisol and Calcisol amended with holm oak biochar: A column study - ScienceDirect. https://www.sciencedirect.com/science/article/pii/S0016706116309867?casa_token=6ehh124M QcMAAAAA:1P1_Wp3v2KomIowBXruQPernCoeO7niq4rg3hzdXGVy0aae3WRWg64UR4Bg 3Yp5VV74RCahVcg.

101.   Apiratikul, R. & Chu, K. H. Improved fixed bed models for correlating asymmetric adsorption breakthrough curves. *Journal of Water Process Engineering* **40**, 101810 (2021).

102.   Nishikawa, E., Cardoso, S. L., Costa, C. S. D., da Silva, M. G. C. & Vieira, M. G. A. New perception of the continuous biosorption of cadmium on a seaweed derivative waste. *Journal of Water Process Engineering* **36**, 101322 (2020).

103.   Nithya, K., Sathish, A. & Kumar, P. S. Packed bed column optimization and modeling studies for removal of chromium ions using chemically modified Lantana camara adsorbent. *Journal of Water Process Engineering* **33**, 101069 (2020).

104.   Lee, C.-G. *et al.* Comparative analysis of fixed-bed sorption models using phosphate breakthrough curves in slag filter media. *Desalination and Water Treatment* **55**, 1795–1805 (2015).

105.   Continuous Fixed-Bed Column Study and Adsorption Modeling: Removal of Lead Ion from Aqueous Solution by Charcoal Originated from Chemical Carbonization of Rubber Wood Sawdust. https://www.hindawi.com/journals/jchem/2015/907379/.

106.   Zhang, W. *et al.* Removal of methylene blue from aqueous solutions by straw based adsorbent in a fixed-bed column. *Chemical Engineering Journal* **173**, 429–436 (2011).

107.   SOME ASPECTS OF THE BEHAVIOR OF CHARCOAL WITH RESPECT TO CHLORINE.1 | Journal of the American Chemical Society. https://pubs.acs.org/doi/pdf/10.1021/ja01448a018.

108.   Heterogeneous Ion Exchange in a Flowing System | Journal of the American Chemical Society. https://pubs.acs.org/doi/pdf/10.1021/ja01238a017.

109. Wan Ngah, W. S., Teong, L. C., Toh, R. H. & Hanafiah, M. A. K. M. Utilization of chitosan–zeolite composite in the removal of Cu(II) from aqueous solution: Adsorption, desorption and fixed bed column studies. *Chemical Engineering Journal* **209**, 46–53 (2012).

110. YOON, Y. H. & NELSON, J. H. Application of Gas Adsorption Kinetics I. A Theoretical Model for Respirator Cartridge Service Life. *American Industrial Hygiene Association Journal* **45**, 509–516 (1984).

111. Hauchhum, L. & Mahanta, P. Carbon dioxide adsorption on zeolites and activated carbon by pressure swing adsorption in a fixed bed. *Int J Energy Environ Eng* **5**, 349–356 (2014).

112. Yang, K. *et al.* Preparation of high surface area activated carbon from coconut shells using microwave heating. *Bioresource Technology* **101**, 6163–6169 (2010).

113. Kamada, Y. *et al.* Wet friction materials for continuous slip torque converter clutch – Fuel economy improvement of passenger cars equipped with automatic transmission –. in *Tribology Series* (eds. Dowson, D. et al.) vol. 34 527–533 (Elsevier, 1998).

114. (PDF) Combustion synthesis of porous MgO and its adsorption properties. *ResearchGate* doi:10.1007/s40090-019-0174-7.

115. Khraisheh, M. *et al.* An overview on trace CO2 removal by advanced physisorbent materials. *Journal of Environmental Management* **255**, 109874 (2020).

116. Li, Y., Yi, H., Tang, X., Li, F. & Yuan, Q. Adsorption separation of CO2/CH4 gas mixture on the commercial zeolites at atmospheric pressure. *Chemical Engineering Journal* **229**, 50–56 (2013).

117. Siriwardane, R. V., Shen, M.-S., Fisher, E. P. & Poston, J. A. Adsorption of CO2 on Molecular Sieves and Activated Carbon. *Energy Fuels* **15**, 279–284 (2001).

118. Walton, K. S., Abney, M. B. & Douglas LeVan, M. CO2 adsorption in Y and X zeolites modified by alkali metal cation exchange. *Microporous and Mesoporous Materials* **91**, 78–84 (2006).

119. Abdullah, A., Idris, I., Shamsudin, I. K. & Othman, M. R. Methane enrichment from high carbon dioxide content natural gas by pressure swing adsorption. *Journal of Natural Gas Science and Engineering* **69**, 102929 (2019).

120. Samanta, A., Zhao, A., Shimizu, G. K. H., Sarkar, P. & Gupta, R. Post-Combustion CO2 Capture Using Solid Sorbents: A Review. *Ind. Eng. Chem. Res.* **51**, 1438–1463 (2012).

121. Ferella, F., Puca, A., Taglieri, G., Rossi, L. & Gallucci, K. Separation of carbon dioxide for biogas upgrading to biomethane. *Journal of Cleaner Production* **164**, 1205–1218 (2017).

122.   de Andrés, J. M., Orjales, L., Narros, A., de la Fuente, M. del M. & Rodríguez, M. E. Carbon dioxide adsorption in chemically activated carbon from sewage sludge. *Journal of the Air & Waste Management Association* **63**, 557–564 (2013).

123.   Kasikamphaiboon, P. & Khunjan, U. CO_2 Adsorption from Biogas Using Amine-Functionalized MgO. *International Journal of Chemical Engineering* **2018**, e1706405 (2018).

124.   Dunstan, M. T., Donat, F., Bork, A. H., Grey, C. P. & Müller, C. R. CO2 Capture at Medium to High Temperature Using Solid Oxide-Based Sorbents: Fundamental Aspects, Mechanistic Insights, and Recent Advances. *Chem. Rev.* **121**, 12681–12745 (2021).